ISSN 1063-7788, Physics of Atomic Nuclei, 2011, Vol. 74, No. 1, pp. 19–39. © Pleiades Publishing, Ltd., 2011.
Original Russian Text © B.S. Ishkhanov, V.N. Orlin, 2011, published in Yadernaya Fizika, 2011, Vol. 74, No. 1, pp. 21–41.

NUCLEI
Theory

Combined Model of Photonucleon Reactions

B. S. Ishkhanov and V. N. Orlin*

Skobeltsyn Institute of Nuclear Physics, Moscow State University, Moscow, 119991 Russia

Received July 1, 2010

Abstract—A combination of the semimicroscopic, exciton, and evaporation models is used to describe photonucleon reactions induced in medium-mass and heavy nuclei by photons of energy below the meson-production threshold. Two mechanisms of the photoexcitation of nuclei are considered. These are the formation of a giant dipole resonance (GDR) at energies in the range $E_\gamma \lesssim 30$ MeV and quasideuteron photoabsorption, which is dominant at energies in the region $E_\gamma \gtrsim 40$ MeV. The densities of particle–hole states appearing in the exciton model are calculated on the basis of the Fermi gas model. Our combined model takes into account the multiparticle emission of preequilibrium particles. The influence of isospin conservation and collective phenomena on photonucleon emission by giant dipole resonances is considered. The combined model is used to describe cross sections for photonucleon reactions proceeding on the ^{40,48}Ca, ^{90}Zr, ^{139}La, ^{142}Nd, and ^{181}Ta nuclei, as well as difference ($E_{\gamma\max} = 85$–55 MeV) bremsstrahlung photoneutron spectra for the ^{63}Cu, ^{115}In, ^{118}Sn, ^{181}Ta, ^{207}Pb, ^{209}Bi, and ^{235}U nuclei and bremsstrahlung photoproton spectra for the ^{90}Zr nucleus at the energies of $E_{\gamma\max} = 22$, 25, and 34 MeV.

DOI: 10.1134/S1063778811010054

1. INTRODUCTION

According to N. Bohr's concept [1], a nuclear reaction can be broken down approximately into two independent stages: the formation of a compound system and its decay to reaction products. In order to describe various photonucleon reactions following the absorption of a photon of energy E_γ by a nucleus, it is therefore necessary to calculate the photoabsorption cross section $\sigma_{\text{abs}}(E_\gamma)$ and to consider all possible or at least the most important nucleon-emission processes at the respective excitation energy of the target nucleus.

Up to the pion-production threshold, photoabsorption on a nucleus is determined by photon interaction only with one- and two-nucleon nuclear currents [2, 3]. In the first case, it is assumed that only one nucleon is excited upon photon absorption. This process is dominant in the region of low energies ($E_\gamma \lesssim 30$ MeV), where an electric giant dipole resonance (GDR), which is a coherent mixture of single-particle–single-hole ($1p1h$) $E1$ excitations, is formed owing to the interaction of the target nucleus with the respective radiation. In the region $E_\gamma \gtrsim 40$ MeV above the giant resonance, the quasideuteron (QD) photoabsorption mechanism becomes dominant. According to this mechanism, the excited nucleon exchanges a virtual pion with a neighboring nucleon, with the result that it is a correlated proton–neutron pair rather than a single nucleon that receives the energy and momentum from the absorbed photon.

For medium-mass and heavy nuclei, basic features of the GDR structure can reliably be calculated on the basis of the semimicroscopic model used in [4–7]. The underlying idea of this model is that collective vibrations of the system of nucleons moving in the mean single-particle potential arise because of their interaction with one another through a single-particle vibrational field formed upon the generation of doorway $1p1h$ excitations, and one can take this into account by introducing separable two-body forces of respective multipolarity. Within this model, the use of a deformed single-particle potential can make it possible to take into account dominant factors that affect the formation of the gross structure of the cross section for $E1$ photoabsorption in medium-mass and heavy nuclei—that is, the deformation [8, 9] and isospin [10, 11] splitting of giant dipole resonances. In order to obtain the cross section for dipole photoabsorption, it is also necessary to estimate the widths of collective dipole states. This can be done either with the aid of phenomenological relations obtained from an analysis of experimental data or on the basis of preequilibrium models of decay of excited nuclear states [12–25].

The quasideuteron component of the photoabsorption cross section can be found within the refined version [3, 26] of the Levinger quasideuteron model [27, 28].

*E-mail: orlinvn@yandex.ru

In describing nucleon emission following photoabsorption, one usually employs the combination of the evaporation and preequilibrium models of photonucleon reactions. There are many different formulations of the preequilibrium approach. However, only semiclassical preequilibrium models (exciton model [12–15] and hydrid model [16–18]) and quantum multistep models [19–25] are used in practice. Quantum models, in which the nucleon-emission probability is defined in terms of quantum-mechanical transition amplitudes, describe better than semiclassical models angular distributions of reaction products. However, this drawback of semiclassical models is compensated to a considerable extent by the simplicity of their application and by their high predictive power in describing nucleon spectra and total reaction cross sections. In view of this, they are still widely used in specific calculations [29, 30].

In the present study, we formulate a combined model of photonucleon reactions on medium-mass and heavy nuclei. In order to describe photoabsorption processes, the semimicroscopic GDR model [4, 7] and the refined quasideuteron model [26] are used in it. Photonucleon emission is described within the exciton model featuring Fermi gas densities of ph states [31] and the evaporation model based on the formulas proposed for nuclear-level densities by Gilbert and Cameron [32]. Some corrections that make it possible to take into account special features of the giant-dipole-resonance reaction channel, such as the collective nature of the doorway $1p1h$ state [33] and the influence of isospin phenomena [34], were introduced in the exciton model [31]. Both affect substantially photonucleon reactions in the giant-dipole-resonance region; for example, the collectivization of the doorway $1p1h$ state increases its lifetime, thereby facilitating the emission of more energetic primary photonucleons, while isospin conservation leads to a predominant decay of the $T_>$ component of the giant dipole resonance through the proton channel.

The combined model is employed here to calculate cross sections for photoneutron and photoproton reactions of various multiplicity on the ^{40,48}Ca, ^{90}Zr, ^{139}La, and ^{142}Nd nuclei in the energy range $E_\gamma \lesssim 40$ MeV and cross sections for photoneutron reactions on the ^{181}Ta nucleus in the energy range $7 \lesssim E_\gamma \lesssim 140$ MeV, as well as total bremsstrahlung spectra for the endpoint energies of $E_{\gamma\max} = 22$, 25, and 34 MeV for the ^{90}Zr nucleus and difference neutron bremsstrahlung spectra for the endpoint bremsstrahlung energies of 55 and 85 MeV for the ^{63}Cu, ^{115}In, ^{118}Sn, ^{181}Ta, ^{207}Pb, ^{209}Bi, and ^{235}U nuclei. Only one free parameter was used in the calculations. This was the ground-state deformation of the target nucleus, and it was estimated on the basis of spectroscopic data. The remaining parameters were taken (after the respective normalization of exciton states) from the GNASH code (Los Alamos) [35]. The results will be compared with experimental data.

2. PHOTOABSORPTION CROSS SECTION

2.1. Semimicroscopic Giant-Dipole-Resonance Model

Electric dipole vibrations arise as a response of the nucleon system to a time-dependent electric field, which induces a dipole moment in a nucleus (vibrational dipole field); that is,

$$F_0 = \sum_{i=1}^{A} (2t_z x)_i,$$

where x is the projection of the nucleon radius vector onto the direction of vibrations and $t_z = \pm 1/2$ is the z component of the nucleon isospin.

The operator F_0 can be treated as one of the components of the total isovector dipole field; that is,

$$F_\mu = \sum_{i=1}^{A} (2t_\mu x)_i \tag{1}$$
$$= \sum_{\alpha>\beta} \Big(\langle\alpha|2t_\mu x|\beta\rangle a_\alpha^+ a_\beta + (-1)^\mu \langle\alpha|2t_{-\mu} x|\beta\rangle a_\beta^+ a_\alpha \Big),$$

where

$$t_\mu = \begin{cases} -(t_x + it_y)/\sqrt{2} & \text{at } \mu = +1, \\ t_z & \text{at } \mu = 0, \\ +(t_x - it_y)/\sqrt{2} & \text{at } \mu = -1 \end{cases} \tag{2}$$

are the spherical components of the nucleon isospin; a_α^+ and a_α are, respectively, the nucleon creation and absorption operators in the single-particle states $|\alpha\rangle$ of energy ε_α; and the symbol $\sum_{\alpha>\beta}$ means summation over the single-particle states $|\alpha\rangle$ and $|\beta\rangle$ that satisfy the condition $\varepsilon_\alpha > \varepsilon_\beta$.

The vibrational field in (1) can generate excitation quanta characterized by the isospin of $\tau = 1$ and by the isospin z projections of $\mu = 0, \pm 1$. These quanta describe normal nodes of isovector vibrations of the nucleon system in the case where one disregards their interaction with one another and with the isospin $T_0 = \left|\dfrac{N-Z}{2}\right|$ of the neutron excess in the nucleus. Vibrations for which $\mu = 0$ correspond to an ordinary photoresonance. They are due to $\Delta T_z = 0$ dipole transitions. Modes in which $\mu = \pm 1$ correspond to charge-exchange vibrations of the nucleon system where one proton transforms into a neutron or vice versa ($\Delta T_z = \pm 1$).

The bulk of the intensity of single-particle dipole transitions caused by the operator F_μ is concentrated in a narrow energy interval around the value

$$\varepsilon_\mu = \hbar\omega_x + \mu\left(V_1 \frac{N-Z}{2A} - E_{\rm Coul}\right), \qquad (3)$$

where ω_x is the average frequency of nucleon vibrations in a three-dimensional oscillator potential along the x axis, $V_1 \approx 100$ MeV is the symmetry potential of the nucleus, and $E_{\rm Coul}$ is the average Coulomb energy of one proton [4].

If the energy spread of single-particle dipole transitions is disregarded, then the operator F_μ can be recast into the form

$$F_\mu = f_\mu c_\mu^+ + (-1)^\mu f_{-\mu} c_{-\mu}, \qquad (4)$$

where

$$c_\mu^+ = f_\mu^{-1} \sum_{\alpha>\beta} \langle\alpha|2t_\mu x|\beta\rangle a_\alpha^+ a_\beta \qquad (5)$$

are quasiboson operators of creation of the initial vibrations $c_\mu^+|T_0T_0\rangle$ ($|T_0T_0\rangle$ is the ground state of the target nucleus), $\mu = 0, \pm 1$. These vibrations are excited with the probability

$$f_\mu^2 = {\sum_{\alpha>\beta}}' \langle\alpha|2t_\mu x|\beta\rangle^2, \qquad (6)$$

where summation is performed over all possible induced single-particle dipole transitions.

The vibrations $c_\mu^+|T_0T_0\rangle$ interact with one another through the vibrational field F_μ, and one can describe this with the aid of the Hamiltonian

$$H = \sum_\mu \varepsilon_\mu c_\mu^+ c_\mu + \frac{1}{2}\varkappa \sum_\mu F_\mu^+ F_\mu, \qquad (7)$$

where $\varkappa$ is the dipole–dipole coupling constant.

The Hamiltonian in (7) can be diagonalized by means of the linear canonical transformation

$$\hat{c}_\mu^+ = X_\mu c_\mu^+ - Y_\mu c_{-\mu}, \qquad (8)$$

where the expansion coefficients X_μ and Y_μ satisfy the orthogonality conditions

$$X_\mu^2 - Y_\mu^2 = 1, \qquad (9)$$
$$X_\mu Y_{-\mu} - Y_\mu X_{-\mu} = 0.$$

Upon this transformation, the operators H and F_μ assume the form

$$H = \sum_\mu \hat{\varepsilon}_\mu \hat{c}_\mu^+ \hat{c}_\mu + E_0, \qquad (10)$$

$$F_\mu = \hat{f}_\mu \hat{c}_\mu^+ + (-1)^\mu \hat{f}_{-\mu} \hat{c}_{-\mu}, \qquad (11)$$

where (see [4])

$$\hat{\varepsilon}_\mu = K + 0.5\left[(\varepsilon_\mu - \varepsilon_{-\mu}) + \varkappa(f_\mu^2 - f_{-\mu}^2)\right] \qquad (12)$$

is the energy of a normal-vibration quantum produced by the quasiboson operator $\hat{c}_\mu^+$,

$$\hat{f}_\mu^2 = 0.5(f_\mu^2 - f_{-\mu}^2) \qquad (13)$$
$$+ K^{-1}\left[\varepsilon_0 f_0^2 + \varkappa(f_0^4 - f_\mu^2 f_{-\mu}^2)\right]$$

is the probability for the excitation of such a quantum,

$$K \equiv \left[(\varepsilon_0 + \varkappa f_0^2)^2 - \varkappa^2 f_\mu^2 f_{-\mu}^2\right]^{1/2}, \qquad (14)$$

and E_0 is the ground-state energy of the nucleus (a constant immaterial for our further consideration).

The total isospin T of the nucleus is approximately an integral of motion, whence it follows that, in nuclei featuring a neutron excess ($T_0 \neq 0$), the absorption of a quantum of the isovector field F_μ having an isospin of $\tau = 1$ must lead to the emergence of states having isospins of $T = T_0 + 1$, T_0, and $T_0 - 1$. In general, the states $|\Phi_\mu\rangle \equiv \hat{c}_\mu^+|T_0T_0\rangle$ do not satisfy this requirement, since they are eigenfunctions of the Hamiltonian in (7), which does not commute with the isospin operator $\mathbf{T}$. These states describe dipole vibrations characterized by a specific z projection of the isospin, $T_z = T_0 + \mu$, but, with the exception of $\mu = +1$ vibrations (which are characterized by the quantum numbers of $T_z = T_0 + 1$ and $T = T_0 + 1$), they are not total-isospin eigenfunctions. This means that the states $|\Phi_\mu\rangle$ characterized by $\mu = 0$ and -1 involve components having different values of the isospin T. In particular, the state $|\Phi_0\rangle$ corresponding to the photoresonance involves components of isospin $T_< \equiv T_0$ and $T_> \equiv T_0 + 1$; that is,

$$|\Phi_0\rangle = g_0(T_0)|\Psi_0(T_0T_0)\rangle \qquad (15)$$
$$+ g_0(T_0+1)|\Psi_0(T_0+1T_0)\rangle,$$

where $|\Psi_0(T_0T_0)\rangle$ and $|\Psi_0(T_0+1T_0)\rangle$ are the normalized wave functions that describe states whose isospins are $T = T_0$ and $T_z = T_0$ in the former case and $T = T_0 + 1$ and $T_z = T_0$ in the latter case.

We assume that the states $|\Psi_0(T_0T_0)\rangle$ and $|\Psi_0(T_0+1T_0)\rangle$ characterize the $T_<$ and $T_>$ peaks into which the photoresonance $|\Phi_0\rangle$ is split. From (15), it follows that the probabilities for the excitation of these states are determined by the quantities $g_0^2(T_0)$ and $g_0^2(T_0+1)$, which are related by the equation

$$g_0^2(T_0) + g_0^2(T_0+1) = 1. \qquad (16)$$

By using the ordinary technique of rotations in isospin space with the aid of the mutually conjugate operators $T_\pm = T_x \pm iT_y$, which change the z projection of the isospin of a state by ± 1, we obtain

$$T_+|\Phi_0\rangle = \sqrt{2(T_0+1)}g_0(T_0+1) \times |\Psi_0(T_0+1T_0+1)\rangle. \quad (17)$$

From here, it follows that

$$g_0^2(T_0+1) = \frac{1}{2(T_0+1)}\langle T_0T_0|[\hat{c}_0, T_-][T_+, \hat{c}_0^+]|T_0T_0\rangle \approx \frac{1}{2(T_0+1)}\langle T_0T_0|\left[[\hat{c}_0, T_-], [T_+, \hat{c}_0^+]\right]|T_0T_0\rangle, \quad (18)$$

where we have employed the conventional notation for the commutator of operators and have considered that

$$[\hat{c}_0, T_-]|T_0T_0\rangle \approx \sqrt{2}\frac{\hat{f}_{+1}}{\hat{f}_0}\hat{c}_{+1}|T_0T_0\rangle = 0 \quad (19)$$

{in the case of application to low-lying states of the nucleus, we have $f_\mu c_\mu^+ \approx \hat{f}_\mu \hat{c}_\mu^+ \approx F_\mu$ [see Eq. (4) and (11)]; therefore, one can use approximately, for such operators, rules of commutation of an isovector with the isospin operator $\mathbf{T}$}.

Substituting the expansion in (8) into expression (18) and using the normalization conditions in (9), we obtain the following estimate of the probability for the excitation of the $T_>$ component of the photoresonance $|\Phi_0\rangle$:

$$g_0^2(T_0+1) \approx \frac{1}{T_0+1}\frac{f_{+1}^2}{f_0^2}. \quad (20)$$

The state

$$|\Psi_0(T_0+1T_0+1)\rangle = \frac{1}{g_0(T_0+1)\sqrt{2(T_0+1)}}[T_+, \hat{c}_0^+]|T_0T_0\rangle \approx \frac{\hat{f}_{+1}\hat{f}_0^{-1}}{g_0(T_0+1)\sqrt{T_0+1}}\hat{c}_{+1}^+|T_0T_0\rangle \quad (21)$$

[see Eq. (17)] is obtained from the state $|\Psi_0(T_0+1T_0)\rangle$ by means of rotation in isospin space. The energy of the former differs from the energy of the latter ($\approx\hat{\varepsilon}_{+1}$) only because of the change in the Coulomb energy of the nucleus upon the transition of a proton into a neutron. In the Hamiltonian H, the term $-E_{\rm Coul}$, which appears in the expression for the energy of the respective single-particle transition, ε_{+1} [see Eq. (3)], ensures this change in the Coulomb energy. Taking into account this circumstance, we obtain the following expression for the excitation energy of the $T_>$ component of the photoresonance $|\Phi_0\rangle$:

$$E_0(T_0+1) \approx \hat{\varepsilon}_{+1} + E_{\rm Coul}. \quad (22)$$

The average excitation energies of the photoresonance $|\Phi_0\rangle$ and its $T_<$ and $T_>$ components are related by the equation [see Eq. (15)]

$$\mathcal{E}_0 = g_0^2(T_0)E_0(T_0) + g_0^2(T_0+1)E_0(T_0+1). \quad (23)$$

We now equate the mean energy of the unsplit photoresonance to the energy $\hat{\varepsilon}_0$ and then obtain the following approximate expression for estimating the excitation energy of the $T_<$ component of the photoresonance:

$$E_0(T_0) \approx \frac{\hat{\varepsilon}_0 - g_0^2(T_0+1)E_0(T_0+1)}{g_0^2(T_0)}. \quad (24)$$

The oscillator strength of electric dipole vibrations for the chosen direction x is

$$\mathcal{S}_0 = \hat{\varepsilon}_0\hat{f}_0^2 = \varepsilon_0 f_0^2 \approx \frac{\hbar^2}{2M_{\rm red}}A, \quad (25)$$

where we have employed a classical sum rule ($M_{\rm red}$ is the reduced nucleon mass and A is the mass number of the target nucleus).

It is natural to define the strengths of the $T_<$ and $T_>$ peaks as

$$S_0(T_0) = g_0^2(T_0)\mathcal{S}_0, \quad S_0(T_0+1) = g_0^2(T_0+1)\mathcal{S}_0. \quad (26)$$

In this case, both the total strength of dipole vibrations and the position of their centroid remain unchanged; that is,

$$\mathcal{S}_0 = S_0(T_0) + S_0(T_0+1), \quad \mathcal{E}_0 = \frac{1}{\mathcal{S}_0}\sum_{T=T_0}^{T_0+1} E_0(T)S_0(T). \quad (27)$$

The total oscillator strength of dipole vibrations is three times as great as the $\mathcal{S}_0$ value given by expression (25), since there are three independent directions for spatial vibrations. In spherical nuclei, different directions of vibrations are degenerate in energy. In deformed nuclei, this degeneracy is removed. In the following, we restrict ourselves to considering, in addition to spherical nuclei, axisymmetric nuclei, for which it is necessary to discriminate between vibrations along the symmetry axis of the nucleus (axis 3) and vibrations in directions orthogonal to it (along axes 1 and 2).

2.2. Parameters of the Semimicroscopic Model

The single-particle energies ε_α of the states $|\alpha\rangle$ and the dipole–dipole coupling constants $\varkappa_3$ and $\varkappa_1 = \varkappa_2$ corresponding to vibrations along the symmetry axis of the nucleus and in directions orthogonal to it are model parameters.

In order to calculate single-particle states, we used the Nilsson deformed potential [36]. The deformation parameter δ', which is the only variable parameter in this potential, is related to the quadrupole-deformation parameter δ of the nucleus (for its definition, see [4]) by the equation

$$\delta' \approx \delta \Big/ \left(1 + \frac{2}{3}\delta\right). \tag{28}$$

The dipole–dipole coupling constants $\varkappa_s$ for longitudinal ($s = 3$) and transverse ($s = 1$ or 2) vibrations are not equal to each other, as follows, for example, from the theoretical estimate obtained in [4]; that is,

$$\varkappa_s = \frac{V_1}{4A\langle x_s^2\rangle}, \tag{29}$$

where

$$\langle x_s^2\rangle = \langle r^2\rangle \left[1 - \frac{2}{3}\delta(1 - 3\delta_{s3})\right] \tag{30}$$

is the average square of the coordinate x_s of a nucleon in the ground state of the nucleus ($\langle r^2\rangle = \langle x_3^2\rangle + 2\langle x_1^2\rangle$ is the average square of the nucleon radius vector).

The constants $\varkappa_3$ and $\varkappa_1$ were varied in such a way as to ensure that the calculation (i) yielded, for the ratio of the energies of longitudinal and transverse dipole vibrations, $\mathcal{E}_{01}/\mathcal{E}_{03}$ (see [8, 9]),

$$\frac{\mathcal{E}_{01}}{\mathcal{E}_{03}} \approx 0.911\frac{\sqrt{\langle x_3^2\rangle}}{\sqrt{\langle x_1^2\rangle}} + 0.089, \tag{31}$$

a result that would be consistent with the introduced quadrupole-deformation parameter δ and (ii) faithfully reproduced the position of the GDR centroid,

$$E_{dip} = \sum_{s=1,3}(1 + \delta_{s1})\mathcal{E}_{0s}\mathcal{S}_{0s} \Big/ (\mathcal{S}_{03} + 2\mathcal{S}_{01}). \tag{32}$$

For the energy E_{dip}, a semiempirical formula that takes into account the effect of the nuclear-surface diffuseness on the GDR position was obtained in [37] in the form

$$E_{dip} \approx 86A^{-1/3}\theta^{-1}(a/R_0)[\,\mathrm{MeV}], \tag{33}$$

where $R_0 \approx 1.07A^{1/3}$ [fm] is the distance from the center of the nucleus to the locus of points where the density of the nucleus decreases by a factor of two, $a \approx 0.55$ fm is the diffuseness parameter of the nuclear surface, and the function $\theta(\xi)$ is given by

$$\theta(\xi) = \left[\frac{1 + \frac{10}{3}\pi^2\xi^2 + \frac{7}{3}\pi^4\xi^4}{1 + \pi^2\xi^2}\right]^{1/2}. \tag{34}$$

Relations (30)–(34) make it possible to fix unambiguously the coupling constants $\varkappa_3$ and $\varkappa_1 = \varkappa_2$. Thus, only one free parameter remains in the model being considered. This is the deformation parameter δ, which can usually be estimated on the basis of data on electric static quadrupole moments [38] or calculated theoretically [39].

2.3. Dipole Photoabsorption Cross Section

The cross section for GDR formation was approximated by the sum of Lorentzian curves corresponding to various modes of sT vibrations; that is,

$$\begin{aligned}
&\sigma_{\text{giant dipole resonance}}(E_\gamma) \qquad (35)\\
&= \sum_{s=1,3}\sum_{T=T_0}^{T_0+1}(1 + \delta_{s1})\sigma^{(sT)}_{\text{giant dipole resonance}}(E_\gamma)\\
&\approx (1 + \alpha)\frac{8\pi e^2}{3\hbar c}\frac{NZ}{A^2}\sum_{s=1,3}\sum_{T=T_0}^{T_0+1}(1 + \delta_{s1})\\
&\times \frac{E_\gamma^2\Gamma_{0s}(T)S_{0s}(T)}{(E_\gamma^2 - E_{0s}^2(T))^2 + E_\gamma^2\Gamma_{0s}^2(T)},
\end{aligned}$$

where $E_{0s}(T)$ and $S_{0s}(T)$ are, respectively, the energy and oscillator strength of dipole vibrations along the x_s directions, $s = 1$, 3, with isospins of $T = T_0$ and $T_0 + 1$ (see Subsection 2.1) and $\Gamma_{0s}(T)$ is the width of the corresponding resonance (for a spherical nucleus, these quantities are independent of the quantum number s).

The choice of normalization factor in (35) was such that the integrated photoabsorption cross section satisfies the relation

$$\begin{aligned}
&\int_0^\infty \sigma_{\text{giant dipole resonance}}(E_\gamma)dE_\gamma \qquad (36)\\
&\approx (1 + \alpha)60\frac{NZ}{A}\ [\mathrm{MeV\ mb}],
\end{aligned}$$

where $\alpha \approx 0.3$ is a dimensionless parameter that takes into account the effect of exchange currents on the strength of dipole transitions.

The total resonance width is the sum of the spreading width $\Gamma^\downarrow$ caused by the decay of the doorway dipole state to $2p2h$ configurations and the radiative width $\Gamma^\uparrow$ associated with the emission of an excited nucleon. In order to estimate the spreading width of $T_<$ resonances, we can employ the semiempirical formula [37]

$$\Gamma^\downarrow_{0s}(T_0) \approx GI(a_0/R_0)E^2_{0s}(T_0), \tag{37}$$

where

$I(\xi) = [1 - 3\xi(1 + \pi^2\xi^2/3)/(1 + \pi^2\xi^2)]/(1 + \pi^2\xi^2)$

is a dimensionless factor, which determines the dependence of the spreading width on the nuclear-surface diffuseness, and $R_0 = 1.07A^{1/3}$ [fm], $a_0 = 1.00$ fm, and $G = 0.00437$ are the adjustable-parameter values obtained from a fit to the experimental values of the GDR widths and refined in the present study.

It is more difficult to estimate the spreading widths of $T_>$ resonances since reliable experimental data for such resonances are scanty. In order to estimate these widths, one can employ statistical relations of the exciton model. According to this model, the spreading width of the doorway $1p1h$ state is given by the relation

$$\Gamma^{\downarrow}_{1p1h}(E) = 2\pi M^2(E)\omega_+(2p2h, E), \quad (38)$$

where $M^2(E)$ is the average square of the two-body transition matrix element and $\omega_+(2p2h, E)$ is the average density of final states accessible in the $1p1h \to 2p2h$ transition (see Subsection 3.1).

In estimating the widths $\Gamma^{\downarrow}_{0s}(T_0 + 1)$, two corrections that take into account the collective nature of the dipole resonance must be introduced in expression (38). Namely, it is necessary to consider that coherent dipole states decay predominantly to $2p2h$ collective states belonging to the *dipole phonon plus surface quadrupole phonon* type, with the result that, in such intranuclear transitions, the maximum energy of the scattered particle or hole decreases by the collective dipole shift. Moreover, such final states do not lie uniformly in the vicinity of the dipole resonance, forming a structure. This leads to a vibrational broadening of the dipole resonance. Upon the introduction of these corrections, the expression for estimating the spreading widths of $T_>$ resonances assumes the form

$$\begin{aligned} &\Gamma^{\downarrow}_{0s}(T_0 + 1) \quad (39) \\ &= 2\pi M^2(E_{0s}(T_0 + 1))\omega_+(2p2h, E_{0s}(T_0 + 1) \\ &- \hat{\varepsilon}_{s,+1} + \varepsilon_{s,+1}) + g^2_{0s}(T_0 + 1)\beta_2 E_{0s}(T_0 + 1), \end{aligned}$$

where β_2 is the amplitude of zero-point quadrupole vibrations of the nuclear surface (for medium-mass nuclei, we have $\beta_2 \sim 0.1$).

The radiative widths $\Gamma^{\uparrow}$ of dipole states can be estimated on the basis of the R-matrix reaction theory (see Subsection 3.6).

2.4. Cross Section for Quasideuteron Photoabsorption

The original quasideuteron model developed by Levinger [27] was refined in [3], where it was proposed to employ, instead of the total cross section for deuteron photodisintegration, only its meson-exchange part, and in [26], where, instead of this, the effect of Pauli blocking on the excitation of a correlated proton—neutron pair in a nucleus was taken into account within the Fermi gas model. Either of the two alternative approaches led to good agreement with experimental data from [40] in the energy range between 20 and 140 MeV (pion-production threshold).

In the present study, we use the approximation [26]

$$\sigma_{\rm QD}(E_\gamma) = L\frac{NZ}{A}\sigma_{\rm D}(E_\gamma)f(E_\gamma), \quad (40)$$

where $L = 6.5$ is the Levinger parameter value,

$$\sigma_{\rm D}(E_\gamma) = 61.2\frac{(E_\gamma - 2.224)^{3/2}}{E^3_\gamma} \quad (41)$$

is a parametrized form of the experimental cross section for deuteron photodisintegration, and

$$\begin{aligned} f(E_\gamma) &= 8.371410^{-2} \quad (42) \\ &- 9.834310^{-3}E_\gamma + 4.122210^{-4}E^2_\gamma \\ &- 3.476210^{-6}E^3_\gamma + 9.353710^{-9}E^4_\gamma \end{aligned}$$

is a dimensionless factor (with E_γ in MeV units) that takes into account the Pauli blocking effect in the energy range $20 \le E_\gamma \le 140$ MeV. We have $f(E_\gamma) = \exp(-73.3/E_\gamma)$ for $E_\gamma < 20$ MeV and $f(E_\gamma) = \exp(24.2/E_\gamma)$ for $E_\gamma > 140$ MeV.

3. PREEQUILIBRIUM AND EQUILIBRIUM DECAY IN PHOTONUCLEON REACTIONS

First, we will disregard isospin and collective phenomena that affect the decay properties of dipole modes of nuclear excitations. This will make it possible to describe any photoexcitation mode (including the quasideuteron mode) within a unified formalism. At the end of this section, we will indicate how one can modify this formalism in order to take into account the aforementioned effects and the competition of soft protons and photons.

3.1. Exciton Model

In the exciton model, it is assumed that photon absorption is followed by the formation of the doorway state with the $m = 2$ or $m = 4$ excitons for, respectively, a dipole $1p1h$ excitation or a quasideuteron $2p2h$ excitation of the target nucleus. This primary excitation decays either via excited-nucleon emission ($m \to m - 1$ transition) or, what is more probable, via a $m \to m + 2$ transition to a more complex configuration because of a residual two-body interaction. After that, this scenario is repeated. The $m = m + 2$ or

$m = m - 1$ exciton state produced at the preceding step either emits a nucleon to a continuum ($m \neq 1$) or undergoes the $m \to m + 2$ intranuclear transition, and so on. Owing to intranuclear ($m \to m + 2$) transitions, the excitation energy of the compound system is distributed over an ever greater number of excitons. At the same time, inverse ($m \to m - 2$) transitions caused by the annihilation of one of the particle–hole pairs because of the transfer of its energy to some particle or hole are also possible. These transitions play a minor role as long as the total number of particles and holes in the system is small. However, the probability of such transitions increases gradually as this number grows. Ultimately, the probability of inverse transitions becomes equal to the probability of direct transitions, with the result that the system reaches the state of thermal equilibrium either in the primary or in one of the residual nuclei, whereupon a comparatively long nucleon-evaporation process, which can be described on the basis of the evaporation model, begins. Preequilibrium nucleon emission becomes insignificant long before the equilibration instant (as early as the first reaction stages); therefore, we will disregard inverse transitions in the following.

Because of nucleon emission, exciton states arise in various nuclei. We introduce the numbers dp and dn indicating how many preequilibrium protons and neutrons have escaped from the $\{Z, N\}$ target nucleus before the emergence of an m exciton state characterized by an excitation energy U. By $P(U; dp, dn, m)$, we denote the probability density for the formation of such a state $|U; dp, dn, m\rangle$.

We can write a recursion equation that would relate the probability density for the formation of the state $|U; dp, dn, m\rangle$ to the probability densities for the formation of states decaying to this state; that is,

$$P(U; dp, dn, m) = \hbar \sum_{\substack{m'=m_0 \\ \Delta m'=2}}^{m} \sum_{j=p,n} D(U; dp, dn, m', m) \tag{43}$$

$$\times \int\limits_{U+B_j(dp_j,dn_j)}^{U_{\max}+B_j(dp_j,dn_j)} \frac{P(U_j; dp_j, dn_j, m'+1)\lambda_j(\varepsilon_j, U_j; dp_j, dn_j, m'+1)dU_j}{\Gamma^{\uparrow}(U_j; dp_j, dn_j, m'+1) + \Gamma^{\downarrow}(U_j; dp_j, dn_j, m'+1)},$$

where $m = m_0, \ m_0 + 2, \ldots, \ \bar{m}$. Here, $m_0 = \max(2, 2(dp + dn))$ or $\max(4, 2(dp + dn))$ for, respectively, the giant-dipole-resonance or quasideuteron reaction channels is the minimum number of excitons arising in the $\{Z - dp, N - dn\}$ nucleus, while $\bar{m} = \bar{m}(U)$ is the mean number of excitons in the thermal-equilibrium state of this nucleus. Further, $U_{\max} = E_\gamma - [dp\, m_p + dn\, m_n + M(Z - dp, N - dn) - M(Z, N)]c^2$ is the maximum excitation energy of the $\{Z - dp, N - dn\}$ nucleus; $B_j(dp_j, dn_j)$ is the separation energy for a nucleon of type j (proton or neutron) from the $\{Z - dp_j, N - dn_j\}$ nucleus, with $dp_j \equiv dp - \delta_{jp}$ and $dn_j \equiv dn - \delta_{jn}$; U_j is the excitation energy of this nucleus; $\lambda_j(\varepsilon_j, U_j; dp_j, dn_j, m'+1)$ is the probability density for the decay per unit time of the exciton state $|U_j; dp_j, dn_j, m'+1\rangle$ with the emission of a j-type nucleon of kinetic energy $\varepsilon_j = U_j - U - B_j(dp_j, dn_j)$ into a continuum; $\Gamma^{\uparrow}(U_j; dp_j, dn_j, m'+1)$ is the total radiative width of this state; $\Gamma^{\downarrow}(U_j; dp_j, dn_j, m' + 1)$ is its spreading width associated with ($m' + 1 \to m' + 3$) intranuclear transitions; $P(U_j; dp_j, dn_j, m' + 1)$ is the probability density for the formation of this state; and

$$D(U; dp, dn, m', m) \tag{44}$$

$$= \begin{cases} 1 \quad \text{for } m' = m, \\ \prod\limits_{\substack{n=m' \\ \Delta n=2}}^{m-2} \dfrac{\Gamma^{\downarrow}(U; dp, dn, n)}{\Gamma^{\uparrow}(U; dp, dn, n) + \Gamma^{\downarrow}(U; dp, dn, n)} \\ \text{for } m' \leq m - 2 \end{cases}$$

is the probability that the intranuclear-transition chain that started in our nucleon system from the m'-exciton state reaches the m-exciton stage.

An expression for the radiative-decay rate $\lambda_j(\varepsilon, E; dp, dn, m)$ was obtained by Cline and Blann [12] by using the detailed-balance principle. It has the form

$$\lambda_j(\varepsilon, E; dp, dn, m) \tag{45}$$

$$= \frac{2s+1}{\pi^2\hbar^3} M_{\text{red}} \varepsilon \sigma_j^{\text{inv}}(\varepsilon; dp, dn)$$

$$\times \frac{\omega(U; dp^{(j)}, dn^{(j)}, m-1)}{\omega(E; dp, dn, m)},$$

where s, $M_{\rm red}$, and $\sigma_j^{\rm inv}(\varepsilon; dp, dn)$ are, respectively, the spin, reduced mass, and inverse-reaction cross section for the emission of a j-type nucleon of energy ε; $U = E - B_j(dp, dn) - \varepsilon$ is the excitation energy of the $\{Z - dp^{(j)}, N - dn^{(j)}\}$ residual nucleus; $dp^{(j)} \equiv dp + \delta_{jp}$; $dn^{(j)} \equiv dn + \delta_{jn}$; and $\omega(E; dp, dn, m)$ and $\omega(U; dp^{(j)}, dn^{(j)}, m-1)$ are the densities of, respectively, the m- and $(m-1)$-exciton states between which the $m \to m-1$ transition occurs.

Integrating this expression with respect to the energy ε and performing in it summation over the index j, we obtain the total probability for the decay per unit time of the exciton state $|E; dp, dn, m\rangle$ because of neutron or proton emission to a continuum. The result is

$$\Gamma^{\uparrow}(E; dp, dn, m)/\hbar \tag{46}$$
$$= \sum_{j=n,p} \int\limits_0^{E-B_j(dp,dn)} \lambda_j(\varepsilon, E; dp, dn, m) d\varepsilon.$$

In estimating the intranuclear-transition rates $\Gamma^{\downarrow}(E; dp, dn, m)/\hbar$ within preequilibrium-decay models, use is made of the first order of perturbation theory. This yields [23–25]

$$\Gamma^{\downarrow}(E; dp, dn, m) = 2\pi M^2 \omega_+(E; dp, dn, m), \tag{47}$$

where M^2 is the average square of the two-body transition matrix element and $\omega_+(E; dp, dn, m)$ is the average density of final states accessible in the $m \to m+2$ transitions.

The densities $\omega(E; dp, dn, m)$ and $\omega_+(E; dp, dn, m)$ appearing in expressions (45) and (47) can be calculated on the basis of the Fermi gas model. On one hand, this choice of densities correlates with the method proposed in [26] for estimating the parameters of the quasideuteron model of photoabsorption; on the other hand, it permits taking into account the effect of the energy dependence of the densities of single-particle and single-hole states (in particular, the vanishing of the density of single-hole states at energies higher than the Fermi energy of $\varepsilon_{\rm F} \approx 35$ MeV) on the dynamics of preequilibrium-cascade development. The procedure used to calculate Fermi gas densities of particle–hole states is described in [31] (see also the footnote in [34]). The inverse-reaction cross sections $\sigma_p^{\rm inv}(\varepsilon; dp, dn)$ and $\sigma_n^{\rm inv}(\varepsilon; dp, dn)$ [see Eq. (45)] were estimated within the optical model [41].

The average matrix element squared $M^2 = M^2(E)$ for $m \to m+2$ intranuclear transitions was chosen on the basis of data from [35]; that is,

$$M^2 = C\frac{k}{A^3 e} \tag{48}$$

$$\times \begin{cases} \sqrt{\dfrac{e}{7\,MeV}}\sqrt{\dfrac{e}{2\,MeV}} & \text{for } e < 2 \text{ MeV}, \\ \sqrt{\dfrac{e}{7\,MeV}} & \text{for } 2 < e < 7 \text{ MeV}, \\ 1 & \text{for } 7 < e < 15 \text{ MeV}, \\ \sqrt{\dfrac{15\,MeV}{e}} & \text{for } e > 15 \text{ MeV}, \end{cases}$$

where $e \equiv E/m$, $k \approx 130$–160 MeV^3 (in the present study, we use the value of 160 MeV^3), and C is a constant that is used to normalize the Fermi gas densities $\omega_+(E; dp, dn, m)$ to similar densities in the equidistant model at $m = 4$ and $E = 40$ MeV.

The quantity $\bar{m} = \bar{m}(U)$ was determined from the condition requiring that, at the state of thermal equilibrium, the mean energy per exciton be equal to 3/2 of the temperature of the nucleus at a given excitation energy; that is,

$$\frac{U}{\bar{m}} = \frac{3}{2}\left[\frac{d(\ln w(U))}{dU}\right]^{-1}, \tag{49}$$

where $w(U)$ is the density of states in the nucleus under study at an excitation energy U (for the choice of this quantity, see the next section).

At the initial reaction stage, we have $dp = dn = 0$, $U = E_\gamma$, and $P(U; 0, 0, m) = \delta(E_\gamma - U)D(U; 0, 0, m_0, m)$, where $m = m_0, m_0 + 2, \ldots, \bar{m}$ ($m_0 = 2$ or 4 for, respectively, the GDR or quasideuteron reaction channels). The recursion relation in (43) makes it possible to find step by step all of the required probability densities $P(U; dp, dn, m)$.

3.2. Evaporation Model

As was indicated above, the development of the preequilibrium cascade ends up in the formation of the preequilibrium state either in the primary nucleus or in one of the residual nuclei, whereupon the photonucleon-evaporation process begins. We denote by $\mathcal{P}(U; dp, dn)$ the probability density for the attainment of the equilibrium state in the $\{Z - dp, N - dn\}$ nucleus. For the target nucleus, we have $\mathcal{P}(U; 0, 0) = P(U; 0, 0, \bar{m}) = \delta(E_\gamma - U)D(U; 0, 0, m_0, \bar{m})$. The remaining probability densities $\mathcal{P}(U; dp, dn)$ can be found by means of the recursion relation

$$\mathcal{P}(U; dp, dn) = P(U; dp, dn, \bar{m}) \tag{50}$$
$$+ \sum_{j=p,n} \int\limits_{U+B_j(dp_j,dn_j)}^{U_{\rm max}+B_j(dp_j,dn_j)} \mathcal{P}(U_j; dp_j, dn_j)$$
$$\times\, \varepsilon_j \sigma_j^{\rm inv}(\varepsilon_j; dp_j, dn_j) w(U; dp, dn)$$

$$\times \left[\sum_{k=p,n} \int\limits_{0}^{U_j - B_k(dp_j, dn_j)} \varepsilon_k \sigma_k^{\text{inv}}(\varepsilon_k; dp_j, dn_j) \right.$$

$$\left. \times\, w(U_{jk}; dp_j + \delta_{kp}, dn_j + \delta_{kn}) d\varepsilon_k \right]^{-1} dU_j,$$

where $U_{jk} = U_j - B_k(dp_j, dn_j) - \varepsilon_k$ and $w(U; dp, dn)$ is the total level density in the $\{Z - dp, N - dn\}$ nucleus at an excitation energy U; the rest of the notation is identical to that in Eq. (43).

In calculating the total level densities $w(U; dp, dn)$, we used the Gilbert–Cameron composite formula [32], which consists of the formula for a constant nuclear temperature and the Fermi gas function $w \propto \exp(2\sqrt{aU})$. The former and the latter are used at, respectively, low and high excitation energies of the nucleus. For a first approximation, the level-density parameter a is in direct proportion to the mass number A of the nucleus [42], but it undergoes strong deviations from this dependence in the region of magic nuclei. One can take this circumstance into account by introducing the shell correction $S = S(Z) + S(N)$, and this ensures a linear dependence between the ratio a/A and this correction [32]; that is,

$$\frac{a}{A} = \begin{cases} 0.00917S + 0.142 \text{ for spherical nuclei,} \\ 0.00917S + 0.120 \text{ for deformed nuclei.} \end{cases} \quad (51)$$

The shell corrections $S(Z)$ and $S(N)$ are presented in [43, 32].

3.3. Total Photonucleon Cross Sections

From the meaning of the quantities $\mathcal{P}(U; dp, dn)$, it follows that the probability for photoexcitation decay accompanied by the emission of l protons and k neutrons is given by

$$W(lpkn; E_\gamma) = \int\limits_{0}^{\min(B_p(l,k), B_n(l,k))} \mathcal{P}(U; l, k) dU, \quad (52)$$

where $l + k = 1, 2, 3 \ldots$.

Therefore, the total cross section for a photonucleon reaction involving the emission of l protons and k neutrons can be represented in the form

$$\sigma(\gamma, lpkn; E_\gamma) = \sigma_{\text{abs}}(E_\gamma) W(lpkn; E_\gamma). \quad (53)$$

3.4. (γ, xp) and (γ, xn) Spectra Integrated with Respect to Angles

The probability density for the emission of a preequilibrium j-type ($j = p, n$) nucleon of energy ε after the emission of $i = 0, 1, 2, \ldots$ nucleons is given by

$$V_j(\varepsilon, E_\gamma; i) = \hbar \sum_{dp=0}^{i} \int\limits_{B_j(dp,dn)}^{U_{\max}} \sum_{\substack{m'=m_0 \\ \Delta m'=2}}^{\bar{m}-2} \frac{P(U; dp, dn, m') \lambda_j(\varepsilon, U; dp, dn, m') dU}{\Gamma^{\uparrow}(U; dp, dn, m') + \Gamma^{\downarrow}(U; dp, dn, m')}, \quad (54)$$

where $dn \equiv i - dp$.

From here, it follows that the energy spectrum of preequilibrium nucleons that is integrated with respect to angles can be calculated by the formula

$$\frac{d\sigma_j^{pre}(\varepsilon, E_\gamma)}{d\varepsilon} = \sum_{i=0}^{\infty} \frac{d\sigma_j^{pre}(\varepsilon, E_\gamma; i)}{d\varepsilon}, \quad (55)$$

where the index $j = p, n$ determines the type of the emitted nucleon and

$$\frac{d\sigma_j^{pre}(\varepsilon, E_\gamma; i)}{d\varepsilon} = \sigma_{\text{abs}}(E_\gamma) V_j(\varepsilon, E_\gamma; i) \quad (56)$$

is the preequilibrium-spectrum component corresponding to the emission of the primary ($i = 0$), secondary ($i = 1$), etc., nucleon.

The probability density for the emission of an equilibrium j-type nucleon from the $\{Z - dp, N - dn\}$ nucleus can be expressed in terms of the probability densities $\mathcal{P}(U; dp, dn)$ (see Subsection 3.2) as

$$\mathcal{V}_j(\varepsilon, E_\gamma; dp, dn) \quad (57)$$

$$= \int\limits_{B_j(dp,dn)}^{U_{\max}} \mathcal{P}(U; dp, dn) \varepsilon \sigma_j^{\text{inv}}(\varepsilon; dp, dn)$$

$$\times\, w(U - B_j(dp, dn) - \varepsilon; dp^{(j)}, dn^{(j)})$$

$$\times \left[\sum_{k=p,n} \int\limits_{0}^{U - B_k(dp,dn)} \varepsilon_k \sigma_k^{\text{inv}}(\varepsilon_k; dp, dn) \right.$$

$$\times\, w(U - B_k(dp, dn) - \varepsilon_k; dp^{(k)}, dn^{(k)})d\varepsilon_k \Bigg]^{-1} dU,$$

where $j = p, n$; the rest of the notation is given in Subsection 3.1.

Multiplying $\mathcal{V}_j(\varepsilon, E_\gamma; dp, dn)$ by the photoabsorption cross section and performing, after that, summation over dp and dn, we obtain an expression for calculating the energy spectrum for evaporated photonucleons that is integrated with respect to angles. The result is

$$\frac{d\sigma_j^{evap}(\varepsilon, E_\gamma)}{d\varepsilon} \tag{58}$$

$$= \sum_{dp,dn} \sigma_{\text{abs}}(E_\gamma)\mathcal{V}_j(\varepsilon, E_\gamma; dp, dn),$$

where $j = p, n$.

The total proton (γ, xp) and neutron (γ, xn) spectra can be obtained by summing expressions (55) and (58).

3.5. Inclusion of Isospin Effects

It was indicated earlier (see Introduction) that, in considering the GDR channel of photonucleon reactions, it is necessary to take into account isospin effects. This is because the $T_>$ components of the giant dipole resonance decay predominantly via proton emission, since, in view of isospin conservation, only high-lying final-nucleus levels of isospin $T' = T_0' + 1$ (here, T_0' is the isospin of the final nucleus in the ground state) are accessible for the neutron decay channel.

Within the model being considered, one can take into account isospin effects [34] by modifying, for the neutron $T_>$ channel of the reaction, the density of exciton states ($\omega(U; dp, dn, m)$) and the total density of states ($w(U; dp, dn)$) [these densities appear in relations (45), (50) and (57)] with the aid of the substitution $U \to U - \Delta(Z - dp, N - dn)$, where $\Delta(Z - dp, N - dn)$ is the excitation energy of the first level, whose isospin is greater by unity than the isospin of the $\{Z - dp, N - dn\}$ nucleus in the ground state (one assumes that the densities of states vanish when the resulting energy becomes negative). The above substitutions permit taking into account the fact that the densities of $T_>$ states are lower than the total densities of states because of their shift upward along the energy scale by about $\Delta(Z - dp, N - dn)$. We note that, in Eq. (45), it is necessary to change only the density $\omega(U; dp, dn + 1, m - 1)$, since, for the neutron $T_>$ channel of the reaction, the densities $\omega(E; dp, dn, m)$ and the cross section $\sigma_n^{\text{inv}}(\varepsilon; dp, dn)$ decrease in the same proportion in relation to their total values.

3.6. Inclusion of Collective Properties of Doorway Dipole States

The doorway dipole excitation is a coherent mixture of $1p1h$ states. This exerts a substantial effect on its decay properties.

For medium-mass and heavy nuclei, the coefficients in the expansion of the doorway dipole state in $1p1h$ configurations are determined in the first approximation by the matrix elements of the dipole operator; that is,

$$C_{\alpha\beta}(sT) \approx \langle\alpha|2t_\mu x_s|\beta\rangle \Bigg/ \left[\sum_{\alpha'>\beta'} \langle\alpha'|2t_\mu x_s|\beta'\rangle^2\right]^{1/2},$$

where the values of $\mu = 0$ and $\mu = +1$ are associated with, respectively, the $T_<$ and the $T_>$ state.

The radiative rate of decay of the dipole sT state can be estimated on the basis of the R matrix theory of nuclear reactions [44]; that is,

$$\lambda_j(\varepsilon, E; 0, 0, 2) \approx \sum_{\alpha>\beta} C^2_{\alpha\beta}(sT) \tag{59}$$

$$\times \frac{\hbar^2 k P_\alpha(k)}{M_{\text{red}}} \frac{\varphi_\alpha^2(\mathcal{R})\mathcal{R}^2}{\int_0^{\mathcal{R}} \varphi_\alpha^2(r) r^2 dr} w_\beta(U),$$

where $j = p, n$ is the emitted-nucleon type, E is the excitation energy of the nucleus, $k = \sqrt{2M_{\text{red}}\varepsilon}$ is the momentum of the outgoing nucleon, ε is its kinetic energy, $U = E - B_j(0, 0) - \varepsilon$ is the excitation energy of the residual nucleus, $P_\alpha(k)$ is the barrier penetrability for the particle $|\alpha\rangle$, $\mathcal{R} = 1.55$ fm is the radius of the nucleon reaction channel, $\varphi_\alpha(r)$ is the radial wave function for the particle $|\alpha\rangle$, and

$$w_\beta(U) = \frac{2}{\pi} \frac{gU^2}{[U^2 - (\varepsilon_\beta^{-1})^2]^2 + g^2U^2} \tag{60}$$

is a function that characterizes the density of smearing of the hole state $|\beta^{-1}\rangle$ of the residual nucleus with energy ε_β^{-1} because of its interaction with other degrees of freedom (g is the width of this smearing as determined from the optical model).

We have already indicated [see Subsection 2.3] that, in the decay of a coherent dipole state to $2p2h$ configurations, there is a trend toward the conservation of the collectivization energy, and this leads to a decrease in the maximum energy of the scatterer particle or hole by the collective dipole shift $\Delta E_{sT} \approx \hat{\varepsilon}_{s\mu} - \varepsilon_{s\mu}$ (where $\mu = 0$ and $\mu = +1$ are approximately associated with $T = T_0$ and $T = T_0 + 1$, respectively) and, hence, to a decrease in the spreading width of the dipole state [see formula (39)]. It is also necessary to take additionally into account the fact that the degree of collectivization of a dipole

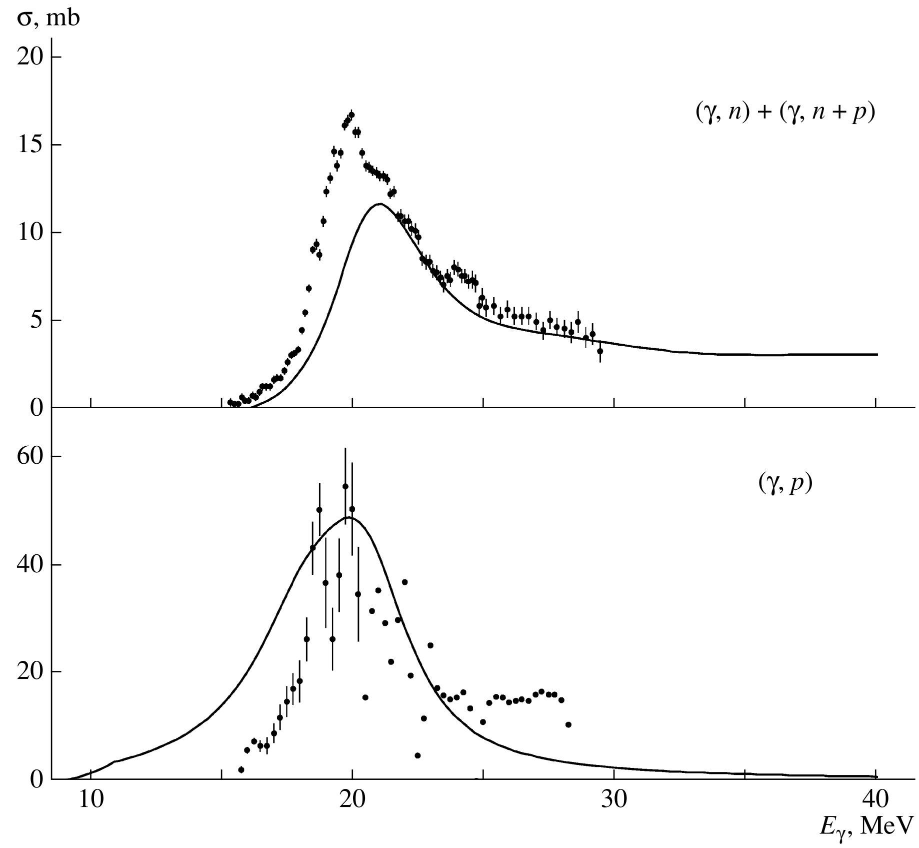

Fig. 1. Cross sections for the $(\gamma, n) + (\gamma, n+p)$ and (γ, p) photonucleon reactions for the ^{40}Ca nucleus in the GDR region. The points with error bars stand for experimental data from [46] for $(\gamma, n) + (\gamma, n+p)$ and [47] for (γ, p). The curves represent the total cross section calculated theoretically.

state [it can be characterized by the ratio $R_{sT}(E) \equiv \sigma^{(sT)}_{\text{giant dipole resonance}}(E)/\sigma^{(sT)}_{\text{giant dipole resonance}}(E_{0s}(T))$] decreases gradually as we move away from the maximum of the $(E_{0s}(T))$ resonance. At an arbitrary excitation energy E, the spreading width of the dipole sT state can therefore be estimated as

$$\Gamma^{\downarrow}(E;0,0,2) \qquad (61)$$
$$= 2\pi M^2 \omega_+(E - R_{sT}(E)\Delta E_{sT};0,0,2).$$

Owing to a decrease in the spreading width of the doorway state, the probability for the emission of a nucleon (carrying away a large energy) increases at the first stage of the preequilibrium cascade, and this leads to a decrease in the yield of secondary, tertiary, etc., nucleons. In describing photonucleon reactions on nuclei featuring an excess of neutrons or protons, it is necessary to take this effect into account; otherwise, we would obtain exaggerated values of cross sections for reactions involving a multiple yield of photonucleons, since, in this case, the threshold for the separation of several nucleons may lie in the vicinity of the dipole-resonance peak, where a maximum collectivization of doorway states occurs.

3.7. Inclusion of Competition between Soft Protons and Photons

If $B_n(0,0) > B_p(0,0)$, then, in the energy range $B_p(0,0) < E_\gamma < B_n(0,0)$, there arises a strong competition between the proton and photon channels of decay of excited states of the target nucleus.

In the Weisskopf single-particle approximation [45], the probability for the emission per 1 s of EJ (electric) radiation is given by

$$P(EJ) = \epsilon_j^2 \frac{18e^2(J+1)k^{2J+1}}{\hbar J[(2J+1)!!]^2}\frac{R^{2J}}{(J+3)^2}, \qquad (62)$$

where ϵ_j is the effective proton charge (about unity for $J \geq 2$), $k = \omega_\gamma/c$ is the wave vector of the emitted photon, and $R \approx 1.2A^{1/3}$ fm is the radius of the nucleus.

In the energy region being considered, the electromagnetic deexcitation of nuclear excitations proceeds predominantly via numerous $E2$ transitions (involving an admixture of $M1$ radiation) whose energy $\hbar\omega_\gamma$ is about several MeV units. In the following, we therefore consider only such transitions.

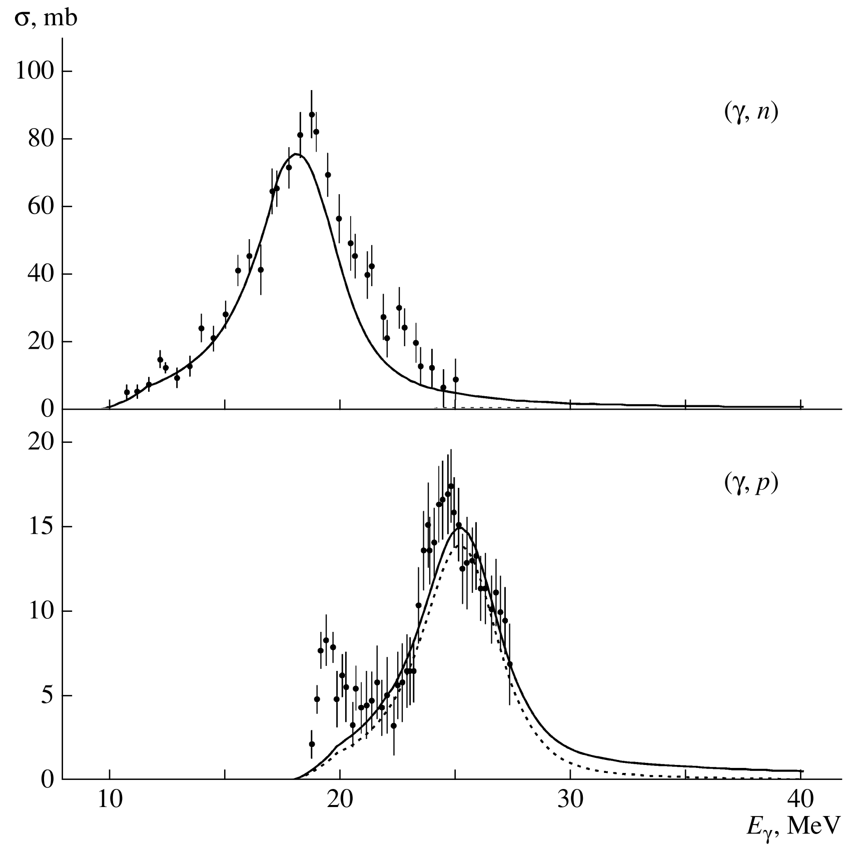

Fig. 2. Cross sections for the (γ, n) and (γ, p) photonucleon reactions on the ^{48}Ca nucleus in the GDR region. The points with error bars stand for experimental data from [48]. The solid and dotted curves represent the results of the calculations for, respectively, the total cross section and the $T_>$ component of the reaction.

The rate of soft-proton emission can be estimated by using an expression that is similar to expression (45) and in which the densities of exciton states are replaced by the total densities of nuclear states.

The bulk of soft protons are emitted via evaporation from the primary nucleus and residual nuclei. These processes are described by Eqs. (50) and (57). In order to take roughly into account the effect of the photon channel, it is sufficient to set, in these equations, the proton spectra $\varepsilon_p \sigma_p^{\mathrm{inv}}(\ldots) w(\ldots)$ to zero when the proton-emission rate becomes smaller than some critical value, $P_{\mathrm{cr}}(E2)$ and to correspondingly modify the threshold $B_p(l, k)$ in Eq. (52). An analysis of available experimental data reveals that the best agreement between the theoretical and experimental results is attained at $P_{\mathrm{cr}}(E2) \approx 1.5 \times 10^{-10} A^{4/3}$, which corresponds to $E2$ radiation of energy $\hbar\omega_\gamma \approx$ 5 MeV.

4. COMPARISON WITH EXPERIMENTAL DATA

The decay features were calculated individually for each component [see Subsections 2.3, 2.4] of the total photoabsorption cross section. After that, the results obtained in this way were summed and compared with experimental data.

The nuclear deformation parameter used in calculating the structure of giant dipole resonances was estimated on the basis of data on static quadrupole moments of nuclei [38].

4.1. Cross Sections for Photonucleon Reactions

^{40,48}Ca. The photoneutron and photoproton cross sections for these calcium isotopes were measured in the energy range $E_\gamma \lesssim 30$ MeV.

In Fig. 1, the cross sections measured in [46, 47] for the $(\gamma, n) + (\gamma, n+p)$ and (γ, p) reactions on the ^{40}Ca nucleus are contrasted against their calculated counterparts. This figure shows that, by and large, the calculation reproduces correctly the experimental ratio of the proton and neutron yields in the decay of the giant dipole resonance in ^{40}Ca. A considerable excess of the proton yield above the neutron yield is explained by the fact that, in this nucleus, the proton-separation energy is nearly one-half as large as the neutron-separation energy.

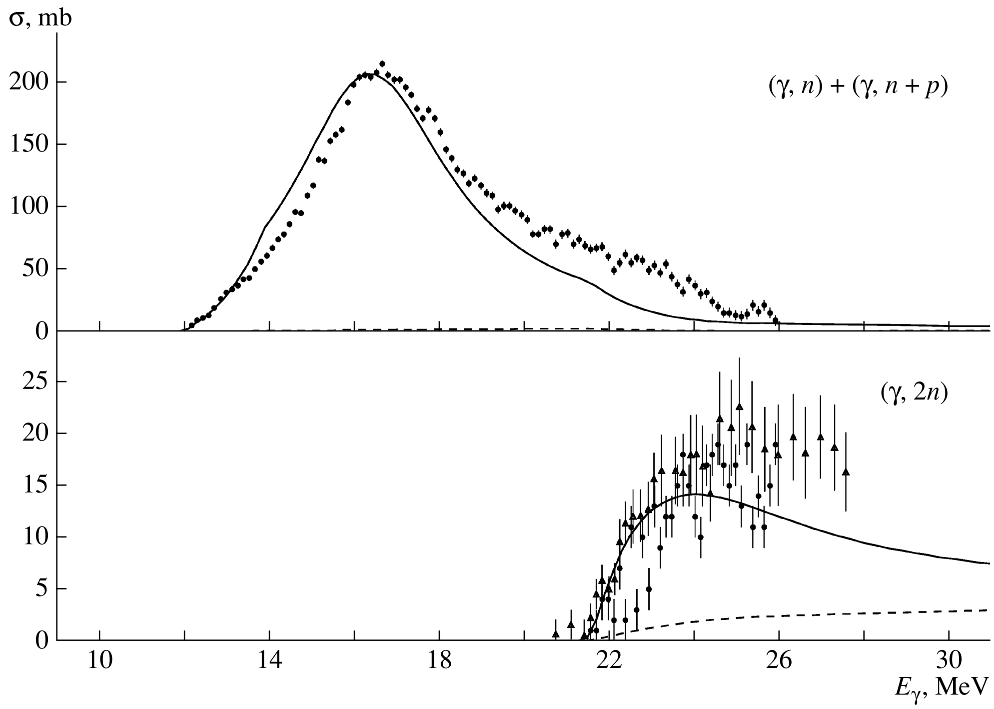

Fig. 3. Cross sections for the $(\gamma, n) + (\gamma, n+p)$ and $(\gamma, 2n)$ photoneutron reactions on the ^{90}Zr nucleus in the GDR region. The points with error bars stand for experimental data from (closed circles) [49] and (closed triangles) [50]. The solid and dashed curves represent the results of the calculations for, respectively, the total cross section and the contribution of the quasideuteron reaction component.

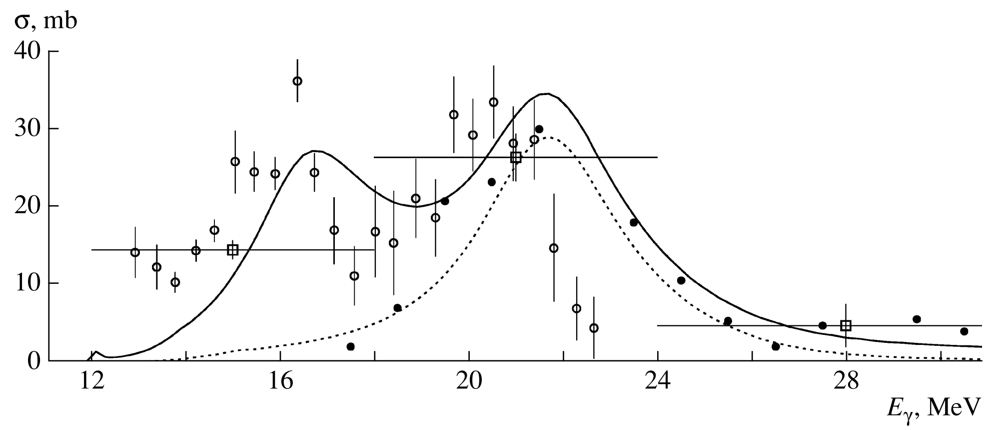

Fig. 4. Cross section for the (γ, p) reaction on the ^{90}Zr nucleus in the GDR region. The displayed points stand for experimental data from (open circels with error bars) [51], (closed circles) [52], and (open boxes with vertical and horizontal errors) [53]. The notation for the curves is identical to that in Fig. 2.

Figure 2 shows data on the cross sections for the reactions ^{48}Ca(γ, n) and ^{48}Ca(γ, p). These experimental data were borrowed from [48]. In contrast to the giant dipole resonance in ^{40}Ca, the giant dipole resonance in ^{48}Ca has two isospin components. The calculation reveals that the $T_>$ component of the giant dipole resonance in ^{48}Ca decays predominantly through the proton channel (the dotted curve in Fig. 2 represents the respective component of the photoproton cross section). This leads to a shift of the maximum of the cross section for the (γ, p) reaction in question by several MeV units toward higher energies with respect to the maximum of the cross section for the respective (γ, n) reaction. There is some disagreement between the theory and experiment at $E_\gamma \sim 20$ MeV: in the experimental cross

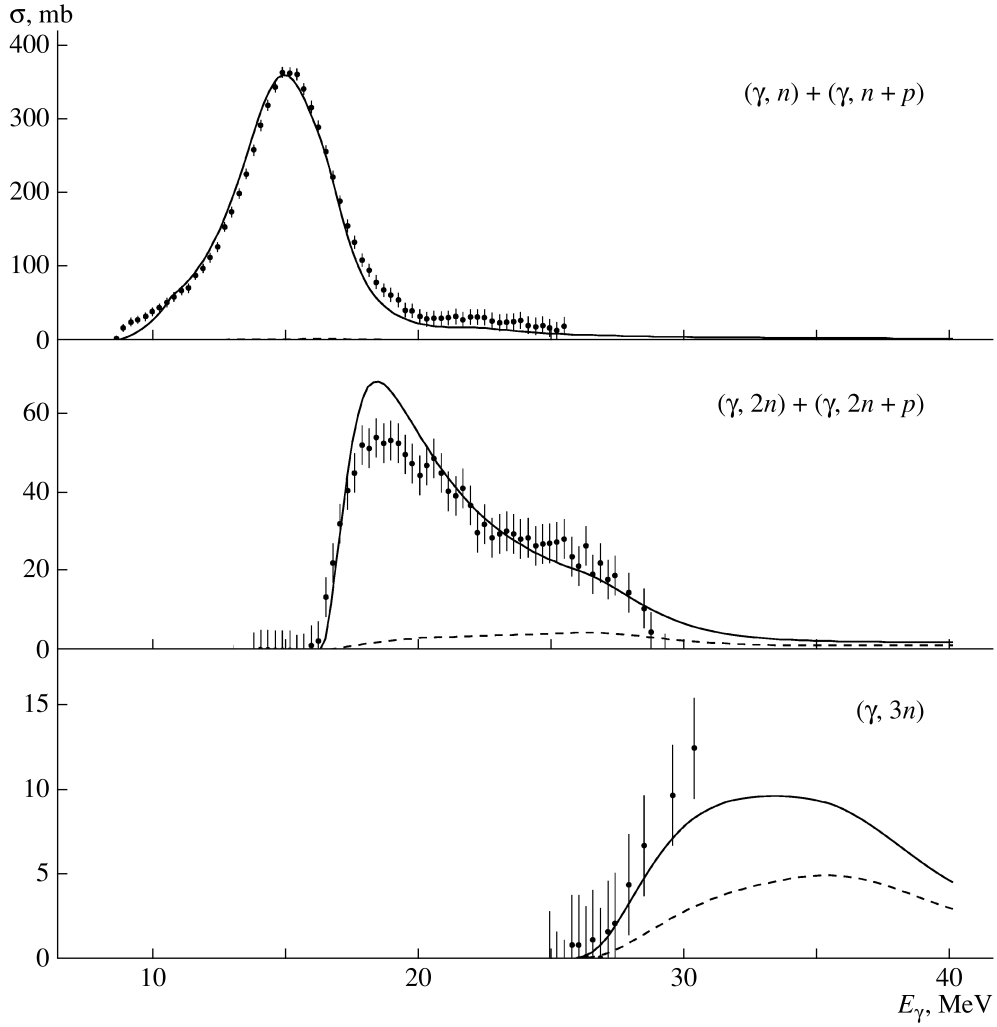

Fig. 5. Cross sections for the $(\gamma, n) + (\gamma, n+p)$, $(\gamma, 2n) + (\gamma, 2n+p)$, and $(\gamma, 3n)$ photoneutron reactions on the ^{139}La nucleus in the GDR region. The points with error bars represent experimental data from [54]. The notation for the curves is identical to that in Fig. 3.

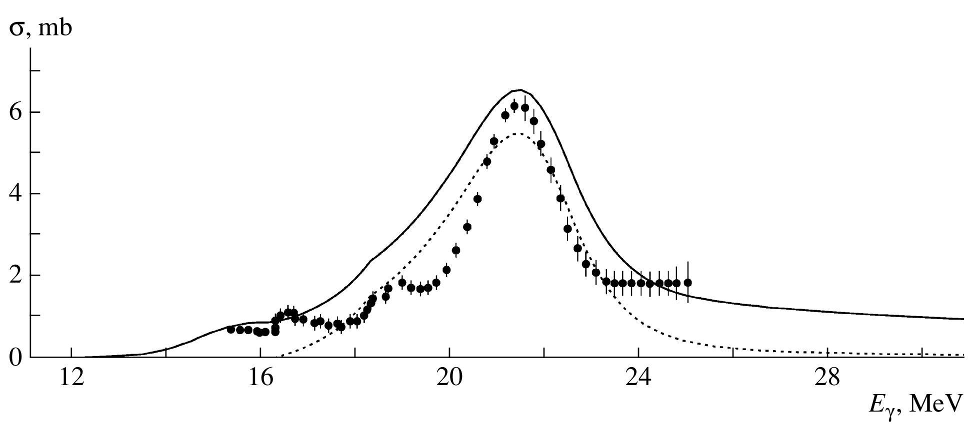

Fig. 6. Cross section for the (γ, p) reaction on the ^{139}La nucleus in the GDR region. The points with error bars represent experimental data from [55]. The notation for the curves is identical to that in Fig. 2.

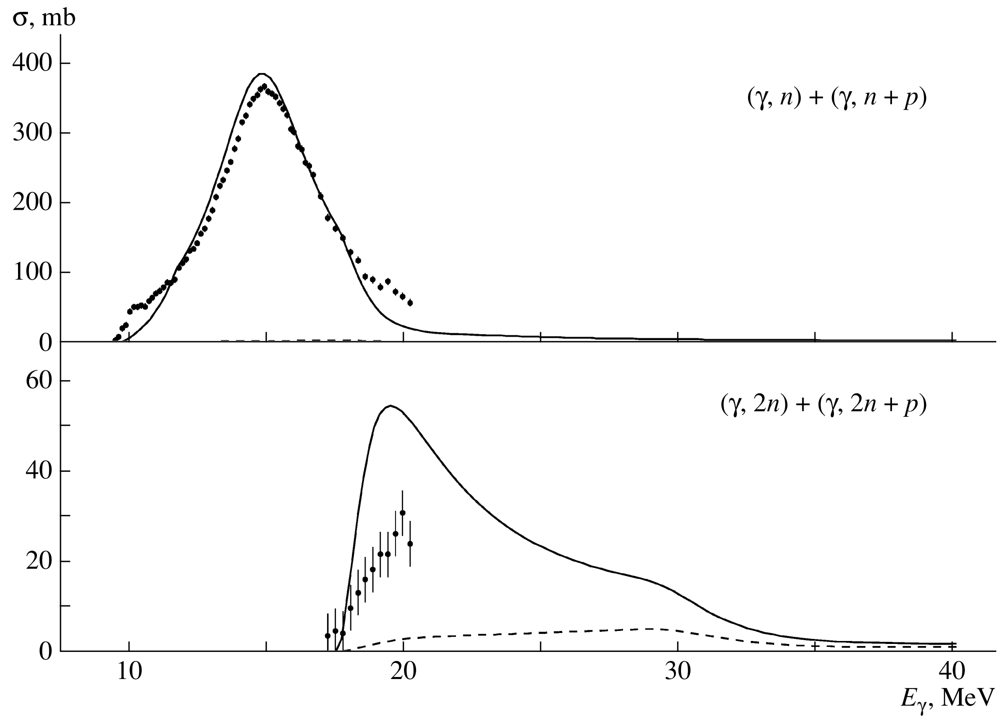

Fig. 7. Cross sections for the $(\gamma, n) + (\gamma, n+p)$ and $(\gamma, 2n) + (\gamma, 2n+p)$ photoneutron reactions on the ^{142}Nd nucleus in the GDR region. The points with error bars represent experimental data from [56]. The notation for the curves is identical to that in Fig. 3.

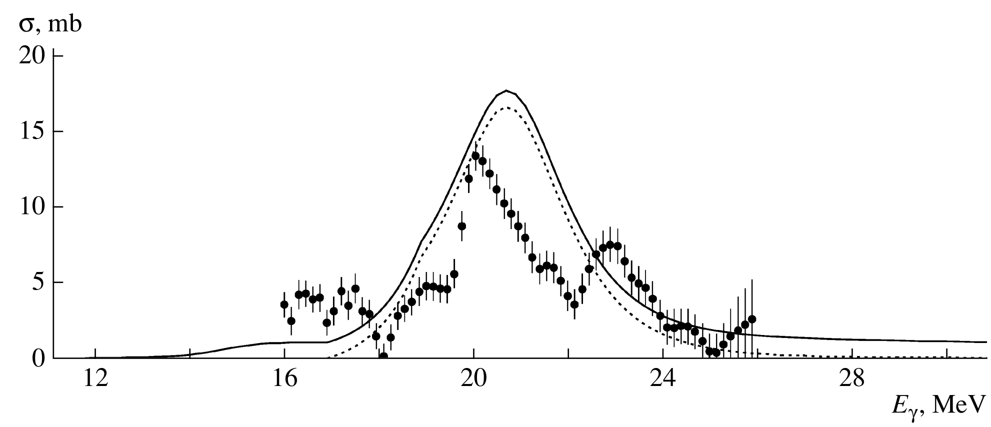

Fig. 8. Cross section for the (γ, p) reaction on the ^{142}Nd nucleus in the GDR region. The points with error bars represent experimental data from [57]. The notation for the curves is identical to that in Fig. 2.

section $\sigma(\gamma, p)$, there is a modest peak corresponding to the $T_<$ branch of the giant dipole resonance. The errors made in the experiment in separating the (γ, n) and (γ, p) yields extracted from the total activation curve measured in a bremsstrahlung-photon beam may be one of the reasons behind this disagreement. We note that the fact that the ratio of the proton- and neutron-separation thresholds for ^{48}Ca is opposite to that for ^{40}Ca leads to a sharp decrease in the amplitude of the cross sections for the reaction $^{48}\mathrm{Ca}(\gamma, p)$.

^{90}Zr. Figure 3 shows the experimental versus calculated cross sections for the $(\gamma, n) + (\gamma, n+p)$ and $(\gamma, 2n)$ reactions on the ^{90}Zr nucleus. The displayed experimental data (points with error bars) were borrowed from [49, 50]. The dashed curve represents the contribution of the quasideuteron reaction channel to the theoretical cross sections. From this figure, one can see that the experimental cross section for the relevant $(\gamma, n) + (\gamma, n+p)$ reaction exceeds substantially its theoretical counterpart in the energy

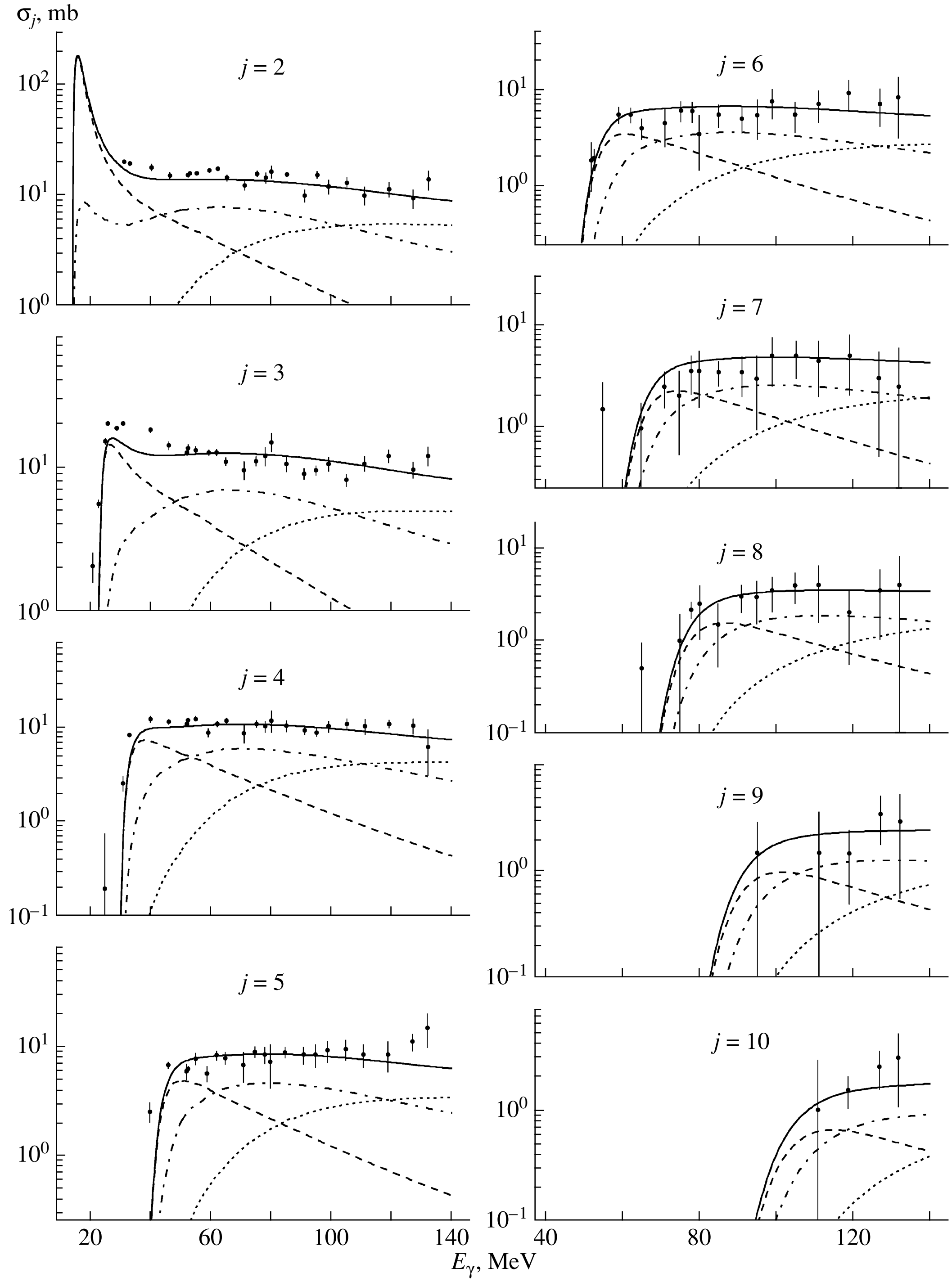

Fig. 9. Cross sections $\sigma_j(E_\gamma)$ for photonucleon reactions induced in ^{181}Ta nuclei and accompanied by the emission of $j, j+1, \ldots$ neutrons and an arbitrary number of charged particles for $15 \lesssim E_\gamma \lesssim 140$ MeV. The points with error bars represent experimental data for a natural-tantalum target from [40]. The curves represent the results of the calculations for (solid curves) the total cross section, (dashed curves) the purely evaporation component of this cross section, (dash-dotted curves) the component involving the emission of one preequilibrium particle, and (dotted curves) the component involving the emission of two preequilibrium particles.

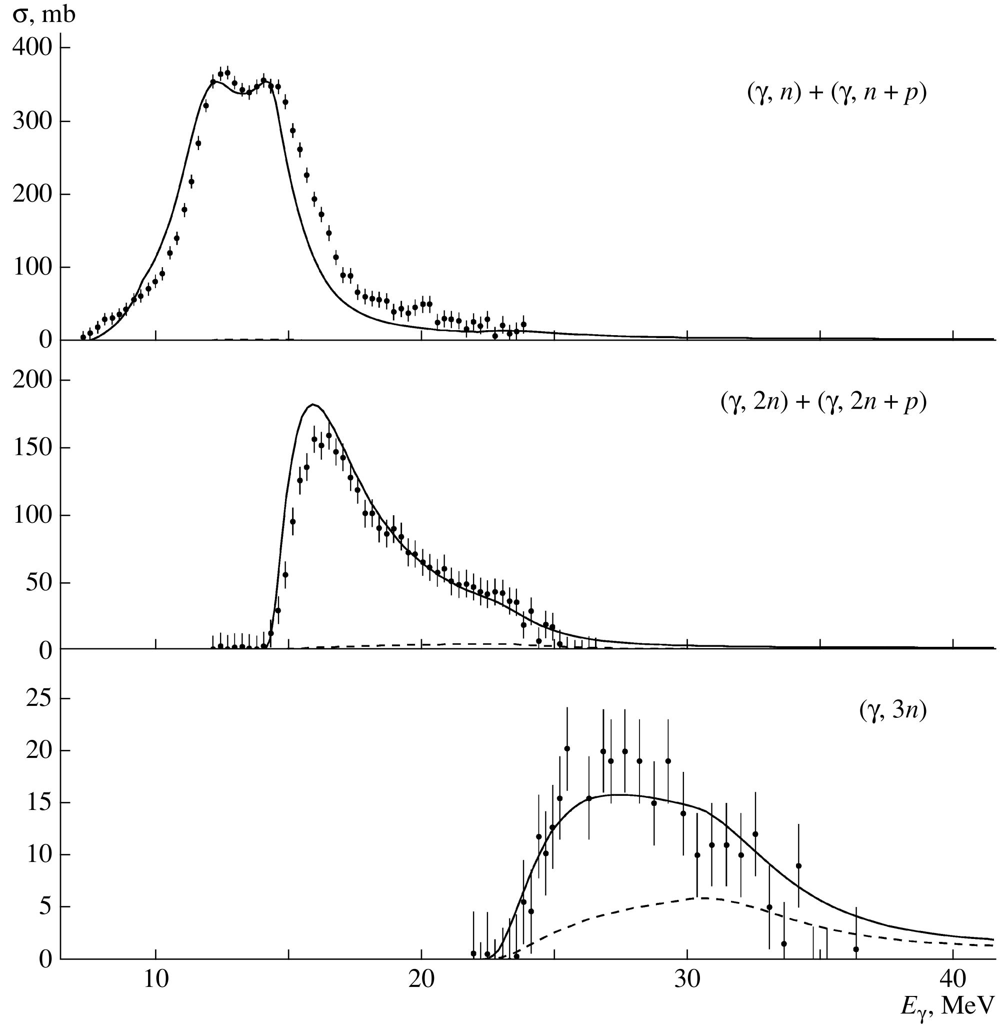

Fig. 10. Cross sections for the $(\gamma, n) + (\gamma, n + p)$, $(\gamma, 2n + p)$, and $(\gamma, 3n)$ photoneutron reactions for the ^{181}Ta nucleus in the GDR region. The points with error bars represent experimental data [54]. The notation for the curves is identical to that in Fig. 3.

region $E_\gamma > 20$ MeV. Possibly, this is due to the contribution to the photoabsorption cross section in this energy region from multipole resonances other than the $E1$ resonance. This could also explain why the experimental data on the cross section $\sigma(\gamma, 2n)$ lie somewhat higher than the respective theoretical results in the energy region $E_\gamma > 24$ MeV.

In Fig. 4, the experimental data on the cross section for the reaction ^{90}Zr(γ, p) from [51–53] are contrasted against the cross section calculated for this reaction. The calculation reproduces satisfactorily experimental data both in the region of the $T_<$ GDR component and in the region of the $T_>$ GDR component. The resonance in the cross section $\sigma(\gamma, p)$ at $E_\gamma \sim 21$–23 MeV is almost completely exhausted by the $T_>$ reaction component (dotted curve in this figure).

^{139}La. The cross sections for the reactions $(\gamma, n) + (\gamma, n + p)$, $(\gamma, 2n) + (\gamma, 2n + p)$, and $(\gamma, 3n)$ in the energy range $E_\gamma \lesssim 30$ MeV [54] (Fig. 5) and the cross section for the reaction (γ, p) [55] (Fig. 6) were measured for this nucleus.

From Fig. 5, one can see that the results of the calculations are more or less consistent with photoneutron experimental data. From the data in Fig. 6, it follows that a dominant contribution to the cross section $\sigma(\gamma, p)$ comes from the $T_>$ reaction component (dotted curve in this figure). The area under the theoretical curve representing $\sigma(\gamma, p)$ is somewhat larger than that under the respective experimental curve.

^{142}Nd. In Fig. 7, we compare the experimental [56] and theoretical cross sections for the reactions ^{142}Nd$((\gamma, n) + (\gamma, n + p))$ and ^{142}Nd$((\gamma, 2n) + (\gamma, 2n + p))$. The accuracy in separating the (γ, n)

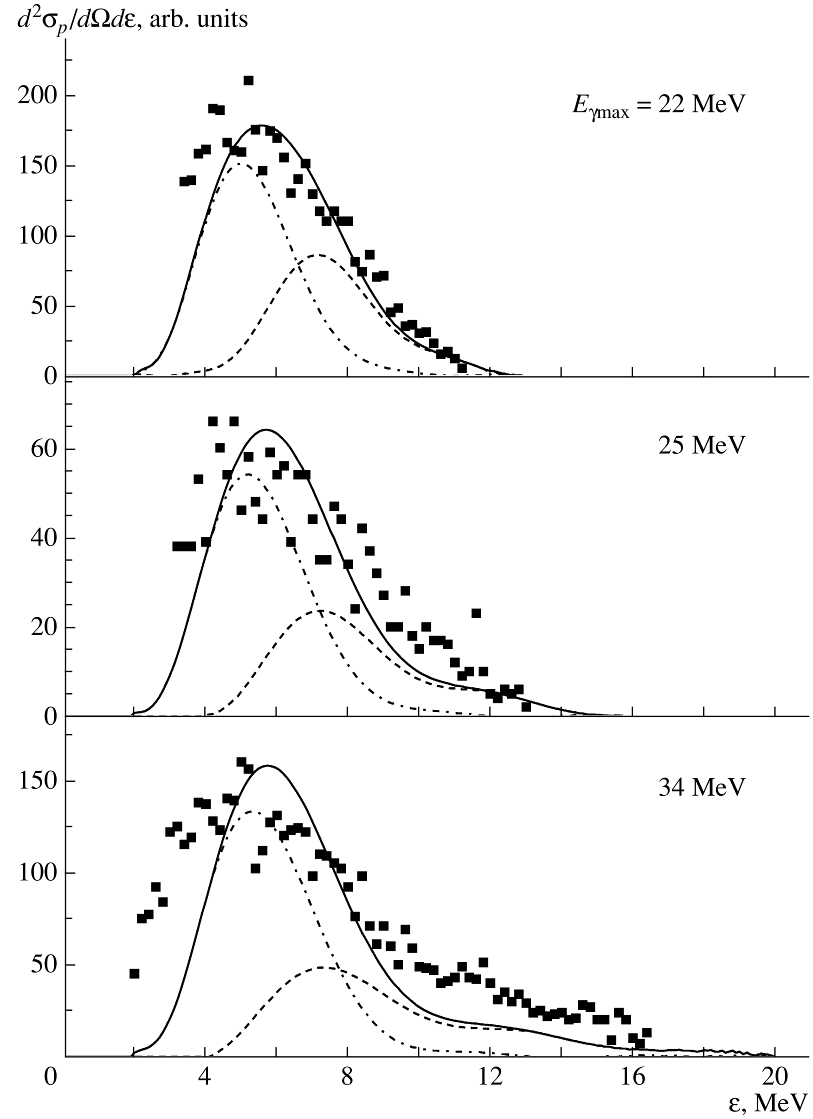

Fig. 11. Experimental photoproton spectra measured in a bremsstrahlung-photon beam at an angle of 90° [58] (closed boxes) and theoretical photoproton spectra integrated over the bremsstrahlung spectrum (curves) for the ^{90}Zr nucleus at the bremsstrahlung-spectrum endpoint energies of $E_{\gamma\max} = 22$, 25, and 34 MeV. The solid, dash-dotted, and dashed curves represent, respectively, the total spectrum, its evaporation component, and its preequilibrium components. Here, ε is the emitted-proton energy.

and $(\gamma, 2n)$ yields is questionable in this case at energies around $E_\gamma \sim 19$–20 MeV (this concerns, first of all, the experiment but also the calculations).

Figure 8 shows the cross section $\sigma(\gamma, p)$ extracted in [57] for the ^{142}Nd nucleus from experimental data on the reaction $^{142}\mathrm{Nd}(e, e'p)$. Our calculation confirms the conclusion drawn in [57] that this cross section is due primarily to the decay of the $T_>$ component of the giant dipole resonance (see dotted curve in Fig. 8).

^{181}Ta. Having performed the separation of different-multiplicity neutron yields, a group from Saclay measured the cross sections $\sigma_j(E_\gamma)$, $2 \leq j \lesssim 10$, for reactions involving the emission into a continuum of j or more neutrons plus any number of charged particles. Those measurements were performed for natural mixtures of isotopes of several nuclei in the energy range 25–132 MeV [40]. In the model being considered, such cross sections can be expressed in terms of the $(\gamma, lpkn)$ cross sections as

$$\sigma_j(E_\gamma) = \sum_{l=0}^{\infty} \sum_{k=j}^{\infty} \sigma(\gamma, lpkn; E_\gamma). \qquad (63)$$

In Fig. 9, the theoretical cross sections $\sigma_j(E_\gamma)$ (solid curves) calculated for the ^{181}Ta nucleus, whose

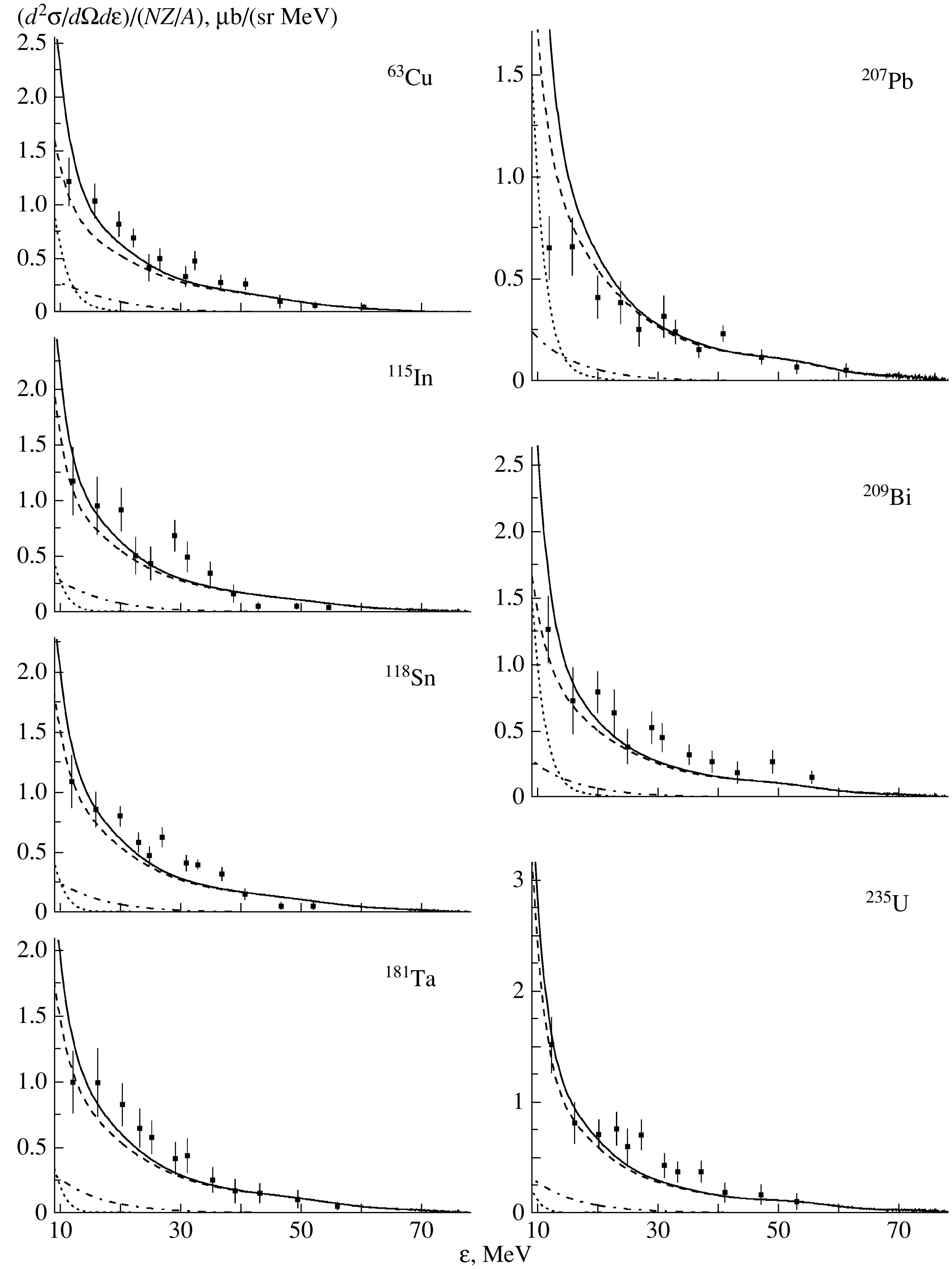

Fig. 12. Difference photoneutron spectra [59] in a bremsstrahlung-photon beam at an angle of 67.5° at the bremsstrahlung-spectrum endpoint energies of $E_{\gamma\max} = 85$ and 55 MeV (points with error bars) and difference theoretical spectra (curves) for the ^{63}Cu, ^{115}In, ^{118}Sn, ^{181}Ta, ^{207}Pb, ^{209}Bi, and ^{235}U nuclei. The solid, dashed, dash-dotted, and dotted curves represent, respectively, the total spectrum, the contribution to it from the first preequilibrium particle, the contribution of the second preequilibrium particle, and the evaporation component of the spectrum. Here, ε is the emitted-neutron energy.

mass number is the closest to the average mass number of natural tantalum targets, are contrasted against experimental data obtained in [40]. On the basis of this comparison, we can conclude that the present model can be used at high values of the energy E_γ. This figure also gives an idea of the contribution to the calculated cross sections from processes not accompanied by preequilibrium-nucleon emission (dashed curves) and accompanied by the emission of one (dash-dotted curves) or two (dotted curves) preequilibrium nucleons.

In Fig. 10, we compare the experimental [54] and theoretical cross sections for the $(\gamma, n) + (\gamma, n+p)$, $(\gamma, 2n) + (\gamma, 2n+p)$, and $(\gamma, 3n)$ reactions on the ^{181}Ta nucleus in the GDR region. By and large, the agreement between the theory and experiment is fairly good, even though the theoretical maximum of the giant dipole resonance is shifted somewhat to the left. This may be the reason why, in Fig. 9, the theoretical cross sections $\sigma_j(E_\gamma)$ are underestimated somewhat in relation to their experimental counterparts in the energy range $E_\gamma \sim 20-40$ MeV.

4.2. Photonucleon Spectra

In the literature, the set of experimental data on the photonucleon energy spectra for medium-mass and heavy nuclei is quite limited, especially for photoproton spectra. Nevertheless, some comparison of theory and experiment can be performed.

Figure 11 shows the proton spectra $d^2\sigma_p(\varepsilon, E_{\gamma\max})/d\Omega d\varepsilon$ measured at an angle of 90° in a bremsstrahlung-photon beam at the bremsstrahlung-spectrum endpoint energies of $E_{\gamma\max} = 22$, 25, and 34 MeV [58]. They are compared (after choosing an appropriate scale factor) with the calculated bremsstrahlung proton spectra

$$[d\sigma_p(\varepsilon, E_{\gamma\max})/d\varepsilon]_{\rm br} = \int\limits_0^{E_{\gamma\max}} [d\sigma_p(\varepsilon, E_\gamma)/d\varepsilon] K(E_\gamma, E_{\gamma\max}) dE_\gamma, \tag{64}$$

where $K(E_\gamma, E_{\gamma\max})$ is a function that is found by the Monte Carlo method and which is taken to approximate the spectrum of the bremsstrahlung used. According to the results of our calculations, the resulting proton spectra can broken down into the low-energy, evaporation (dash-dotted curve), and high-energy, preequilibrium (dashed curve), components. The agreement between the respective theoretical and experimental results deteriorates as the bremsstrahlung-spectrum endpoint energy becomes higher. This may be attributed to the aforementioned deficiency of the theoretical photoabsorption cross section on the ^{90}Zr nucleus in the energy region $E_\gamma > 20$ MeV.

In [59], the difference energy spectra of photoneutrons for bremsstrahlung of endpoint energy $E_{\gamma\max} =$ 85 and 55 MeV,

$$[d^2\sigma_n(\varepsilon)/d\Omega d\varepsilon]_{\rm dif} = \frac{[d^2\sigma_n(\varepsilon, 85)/d\Omega d\varepsilon]_{\rm br} - [d^2\sigma_n(\varepsilon, 55)/d\Omega d\varepsilon]_{\rm br}}{\int_{E_{\rm norm}}^{85} [K(E_\gamma, 85) - K(E_\gamma, 55)] dE_\gamma}, \tag{65}$$

where $K(E_\gamma, E_{\gamma\max})$ is the bremsstrahlung spectrum for a thin tantalum target (it is virtually coincident with Schiff's spectrum [60]) and $E_{\rm norm} = 18$ MeV is the energy at which the two spectra are normalized to the same number of photons, were measured for a number of medium-mass and heavy nuclei (Cu, In, Sn, Ta, Pb, Bi, and U) at an angle of 67.5°.

In Fig. 12, these spectra are contrasted against the calculated difference energy spectra

$$[d\sigma_n(\varepsilon)/d\varepsilon]_{\rm dif} = \frac{[d\sigma_n(\varepsilon, 85)/d\varepsilon]_{\rm br} - [d\sigma_n(\varepsilon, 55)/d\varepsilon]_{\rm br}}{\int_{E_{\rm norm}}^{85} [K(E_\gamma, 85) - K(E_\gamma, 55)] dE_\gamma}, \tag{66}$$

divided by ten 10 (in this case, the agreement between the theoretical and experimental data is somewhat better than in the case of division by 4π). In addition to the total calculated spectrum (solid curve), Fig. 12 also shows its components corresponding to neutron evaporation (dotted curve) and processes involving the emission of the first (dashed curve) and second (dash-dotted curve) preequlibrium particle.

5. CONCLUSIONS

The calculations performed above have shown that our combined model, in which we take into account all basic stages of photonucleon reactions, makes it possible to obtain, for medium-mass and heavy nuclei, a satisfactory description of total cross sections for photonucleon reactions of different multiplicity and the (γ, xp) and (γ, xn) energy spectra integrated with respect to angles. This proved to be possible both in the GDR region and at high values of the energy E_γ (up to the pion-production threshold).

It is important to note that all of the calculations have been performed with the standard set of parameters—that is, no individual fitting for specific nuclei has been performed. This demonstrates a high predictive power of the model.

It is also of importance that, within the same model, we have described simultaneously both photoneutron and photoproton reaction channels. This imposes severe requirements upon the underlying principles of the model.

The results of our calculations are indicative of a strong effect of isospin and collective phenomena in the GDR region on photonucleon reactions (in particular, on the competition between protons and neutrons and on the multiplicity of their yields).

ACKNOWLEDGMENTS

We are grateful to S.Yu. Troshchiev for his help in the preparation of the manuscript for publication.

This work was supported by the Ministry of Education and Science of the Russian Federation (under state contract no. 02.740.11.0242).

REFERENCES

1. N. Bohr, Nature **137**, 344 (1936).
2. J. M. Laget, Nucl. Phys. A **312**, 265 (1978).
3. J. M. Laget, in *Lecture Notes in Physics*, Vol. 137, Ed. by H. Arenhovel and A. M. Saruis (Springer, Berlin, 1981), p. 148.
4. O. Bohr and B. Mottelson, *Nuclear Structure*, vol. 2: *Nuclear Deformations*(Benjamin, New York, 1975; Mir, Moscow, 1977).
5. B. S. Ishkhanov and V. N. Orlin, Yad. Fiz. **66**, 1269 (2003) [Phys. At. Nucl. **66**, 1229 (2003)].
6. B. S. Ishkhanov and V. N. Orlin, Yad. Fiz. **67**, 614 (2004) [Phys. At. Nucl. **67**, 595 (2004)].
7. B. S. Ishkhanov and V. N. Orlin, Fiz. Elem. Chastits At. Yadra **38**, 460 (2007) [Phys. Part. Nucl. **38**, 232 (2007)].
8. M. Danos, Nucl. Phys. **5**, 23 (1958).
9. K. Okamoto, Prog. Theor. Phys. **15**, 75 (1956).
10. S. Fallieros and B. Goulard, Nucl. Phys. A **147**, 593 (1970).
11. R. Ö. Akyüz and S. Fallieros, Phys. Rev. Lett. **27**, 1016 (1971).
12. C. K. Cline and M. Blann, Nucl. Phys. A **172**, 225 (1971).
13. C. K. Cline, Nucl. Phys. A **210**, 590 (1973).
14. E. Gadioli, E. Gadioli Erba, and P. G. Sona, Nucl. Phys. A **217**, 589 (1973).
15. J. Dobes and E. Beták, Nucl. Phys. A **272**, 353 (1976).
16. M. Blann, Phys. Rev. Lett. **27**, 337 (1971).
17. M. Blann, Phys. Rev. Lett. **28**, 757 (1972).
18. M. Blann and H. K. Vonach, Phys. Rev. C **28**, 1475 (1983).
19. H. Feshbach, A. Kerman, and S. Koonin, Ann. Phys. (N.Y.) **125**, 429 (1980).
20. T. Tamura, T. Udagawa, and H. Lenske, Phys. Rev. C **26**, 379 (1982).
21. H. Nishioka et al., Ann. Phys. (N. Y.) **172**, 67 (1986).
22. H. Nishioka, H. A. Weidenmüller, and S. Yoshida, Ann. Phys. (N.Y.) **183**, 166 (1988).
23. J. M. Akkermans and A. J. Koning, Phys. Lett. B **234**, 417 (1990).
24. A. J. Koning and J. M. Akkermans, Ann. Phys. (N. Y.) **208**, 216 (1991).
25. A. J. Koning and M. B. Chadwick, Phys. Rev. C **56**, 970 (1997).
26. M. B. Chadwick et al., Phys. Rev. C **44**, 814 (1991).
27. J. S. Levinger, Phys. Rev. **84**, 43 (1951).
28. J. S. Levinger, Phys. Lett. B **82**, 181 (1979).
29. C. Kalbach, J. Phys. G **21**, 1519 (1995).
30. A. J. Koning and M. C. Duijvestijn, Nucl. Phys. A **744**, 15 (2004).
31. B. S. Ishkhanov and V. N. Orlin, Yad. Fiz. **71**, 517 (2008) [Phys. At. Nucl. **71**, 493 (2008)].
32. A. Gilbert and A. G. W. Cameron, Can. J. Phys. **43**, 1446 (1965).
33. B. S. Ishkhanov and V. N. Orlin, Yad. Fiz. **72**, 2074 (2009) [Phys. At. Nucl. **72**, 2010 (2009)].
34. B. S. Ishkhanov and V. N. Orlin, Yad. Fiz. **72**, 444 (2009) [Phys. At. Nucl. **72**, 410 (2009)].
35. P. G. Young, E. D. Arthur, and M. B. Chadwick, Technical Report No. LA-12343-MS (Los Alamos Nat. Labor., Los Alamos, NM, 1992).
36. S. Nilsson, in *Deformation of Atomic Nuclei,* Ed. by R. Edmonds (Inostr. Liter., Moscow, 1958), p. 232 [in Russian].
37. B. S. Ishkhanov and V. N. Orlin, Yad. Fiz. **66**, 688 (2003) [Phys. At. Nucl. **66**, 659 (2003)].
38. N. Stone, *Table of New Nuclear Moments*, Preprint 1997, a revision of the *Table of Nuclear Moments* by P. Raghavan, At. Data Nucl. Tables **42**, 189 (1989); http://www.nndc.bnl.gov/nndc/stone-moments
39. B. S. Ishkhanov and V. N. Orlin, Yad. Fiz. **68**, 1407 (2005) [Phys. At. Nucl. **68**, 1352 (2005)].
40. A. Lepretre et al., Nucl. Phys. A **367**, 237 (1981).
41. A. J. Koning and J. P. Delaroche, Nucl. Phys. A **713**, 231 (2003).
42. H. A. Bethe, Phys. Rev. **50**, 332 (1936).
43. J. L. Cook et al., Austral. J. Phys. **20**, 477 (1967).
44. A. S. Davydov, *Theory of Atomic Nuclei* (Fizmatgiz, Moscow, 1958) [in Russian].
45. V. F. Weisskopf, Phys. Rev. **83**, 1073 (1951).
46. A. Veyssiere et al., Nucl. Phys. A **227**, 513 (1974).
47. B. I. Goryachev et al., Yad. Fiz. **7**, 944 (1968) [Sov. J. Nucl. Phys. **7**, 567 (1968)].
48. G. J. O'Keefe et al., Nucl. Phys. A **469**, 239 (1987).
49. A. Lepretre et al., Nucl. Phys. A **175**, 609 (1971).
50. B. L. Berman et al., Phys. Rev. **162**, 1098 (1967).
51. D. Brajnik et al., Phys. Rev. C **13**, 1852 (1976).
52. I. I. Dushkov et al., Izv. Akad. Nauk SSSR, Ser. Fiz. **29**, 213 (1965).
53. W. R. Dodge et al., Phys. Rev. C **32**, 781 (1985).
54. R. Bergere et al., Nucl. Phys. A **121**, 463 (1968).
55. K. Shoda, Phys. Rep. **53**, 341 (1979).
56. P. Carlos et al., Nucl. Phys. A **172**, 437 (1971).
57. T. Saito et al., Phys. Rev. C **16**, 958 (1977).
58. I. I. Dushkov et al., Phys. Lett. **10**, 310 (1964).
59. N. N. Kaushal et al., Phys. Rev. **175**, 1330 (1968).
60. L. I. Schiff, Phys. Rev. **83**, 252 (1951).

Translated by A. Isaakyan